

Highlights

A coupled mathematical and numerical model for protein spreading and tissue atrophy applied to Alzheimer's disease

Valentina Pederzoli, Mattia Corti, Davide Riccobelli, Paola F. Antonietti

- Construction of a novel coupled model of the spreading of a tau protein in Alzheimer's disease and brain tissue atrophy
- Definition of an effective numerical approximation based on Discontinuous Galerkin methods for the solution of the model
- Numerical simulations to model the progression and induced brain atrophy typical of Alzheimer's disease

A coupled mathematical and numerical model for protein spreading and tissue atrophy applied to Alzheimer's disease

Valentina Pederzoli^{a,*}, Mattia Corti^a, Davide Riccobelli^{a,b} and Paola F. Antonietti^a

^aMOX-Dipartimento di Matematica, Politecnico di Milano, Piazza Leonardo da Vinci 32, Milan, 20133, Italy

^bMathematics Area, mathLab, SISSA, Via Bonomea 265, Trieste, 34136, Italy

ARTICLE INFO

Keywords:

Fisher-Kolmogorov

Elasticity

Atrophy

Discontinuous Galerkin

ABSTRACT

The aim of this paper is to introduce, analyse and test in practice a new mathematical model describing the interplay between biological tissue atrophy driven by the diffusion of a biological agent, with applications to neurodegenerative disorders. This study introduces a novel mathematical and computational model comprising a Fisher-Kolmogorov equation for species diffusion coupled with an elasticity equation governing mass loss. These equations intertwine through a logistic law dictating the reduction of the medium's mass. This model is applied to the onset and development of Alzheimer's disease. Here, the equations describe the propagation of misfolded τ -proteins and the ensuing brain atrophy characteristic of the disease. To address numerically the inherited complexities, we propose a Discontinuous Galerkin method for spatial discretization, while time integration relies on the Crank-Nicolson method. We present the mathematical model, explore its characteristics, and present the proposed discretization. Furthermore, convergence results are presented to verify the model's implementation, accompanied by simulations illustrating the application scenario of the onset of Alzheimer's disease.

1. Introduction

Population dynamics is increasingly employed in biology to describe the evolution of various phenomena, including the progression of neurodegenerative diseases [44] and the development of tumors [47]. In some cases, the spread of biological agents can cause changes in mass within the affected tissues. The integration of population dynamics systems with models of growth or atrophy allows the description of such phenomena employing coupled multiphysics models. For instance, neurodegenerative diseases arise from the damage and degeneration of the neurons in the regions of the brain associated with cognitive functions [13].

In the context of neurodegenerative diseases, the underlying causes often involve the gradual buildup of damaged protein agglomerations, which cause the eventual degeneration of neurons. After sustaining damage, it is theorized that the protein gains the capacity to migrate between neurons, induce misfolding of other healthy proteins, and aggregate with them [20, 23, 24]. This process is known as *prion-like* behavior and is used to model the spreading of the misfolded proteins. In the literature, we can find different approaches to model protein spreading in neurodegenerative diseases. One major class includes kinetic growth and fragmentation models, which employ a set of ordinary differential equations to study the local interaction of aggregates of different sizes [29]. Alternative approaches employ network diffusion models and graph theory, used to study the diffusion at the organ level[42]. A third widely employed class of approaches builds on reaction-diffusion continuum models, employing systems of partial differential equations[44].

In the literature, this last class of approaches comprises three possible models: the Fisher-Kolmogorov (FK) equation, the Heterodimer model, and the Smoluchowski model [42, 44]. The FK model is a nonlinear reaction-diffusion equation in one variable, modeling the relative concentration of the agent [44, 42, 6, 53]. It is widely used for its simplicity, even though it does not take into account the healthy protein dynamics. The heterodimer model is more complex as it accounts for two different configurations of proteins: healthy and misfolded ones. In this model, the

* VP, MC, and PFA have been funded by the European Union (ERC, NEMESIS, project number 101115663). Views and opinions expressed are however those of the author(s) only and do not necessarily reflect those of the European Union or the European Research Council Executive Agency. The present research is part of the activities of Dipartimento di Eccellenza 2023-2027. DR has been partially supported by PRIN 2022 project *Mathematical models for viscoelastic biological matter*, Prot. 202249PF73 – Funded by European Union - Next Generation EU - Italian Recovery and Resilience Plan (PNRR) - M4C1, CUP D53D23005610001. VP, MC and PFA are members of INdAM-GNCS. DR is member of INdAM-GNFM.

✉ valentina.pederzoli@polimi.it (V. Pederzoli)

ORCID(s):

rates of aggregation and conversion of the proteins are taken into account, as well as the clearance and production of misfolded and healthy proteins [44, 8]. However, this model cannot capture the size of the misfolded proteins aggregate, or their nucleation and fragmentation [42]. Finally, the Smoluchowski model is the more complex approach but allows to study the kinetics of protein aggregates of different sizes [10] while involving a large number of parameters to be calibrated [42].

To study the atrophy of the brain during the development of neurodegenerative diseases, these propagation models can be coupled with a model of loss of mass. The coupling is achieved by introducing a measure of the volume loss, the relative rate of which is somewhat proportional to the total exposure of the tissue to the misfolded proteins [9, 27]. In this work, we introduce a multiphysics model to investigate tissue atrophy driven by the agent spread, with a focus on applications to Alzheimer's disease. Specifically, for the spreading of the misfolded proteins, we adopt an FK model. Indeed, the FK equation is the simplest choice for modeling the problem, and it has already been used in literature of atrophy modelling [9, 53]. The novelty of the model relies on a new constitutive equation for the inelastic component of the stress tensor used to model tissue atrophy. Other works focus on the coupling between FK equation with elasticity, such as [53], where the authors introduced a linear atrophy law. On the contrary, we propose a logistic law, avoiding the eventual decay of tissue mass to zero.

In literature, numerical implementations commonly use a continuous finite element method (FEM). Another approach can be found in [6, 8], which employs the discontinuous Galerkin (DG) method on polyhedral meshes. DG methods provide numerous advantages with respect to the classical conforming FEM formulations. First, it empowers us to adjust approximation parameters locally, such as the polynomial degree p and the element diameter h . This feature enables the easy handling of meshes with non-conforming elements [34], which is impossible when employing continuous finite elements. Additionally, the DG method allows the possibility of using polygonal mesh elements, which could be incredibly useful in brain applications, where the irregularity of the domain boundary and internal interfaces require the use of a large number of faces to guarantee an appropriate description. Due to these advantages, particularly connected with the proposed application field, we propose a DG discretization approach for the space discretization of our model. The proposed method is coupled with the Crank-Nicolson method for time integration, and we consider a semi-implicit approach to treat the nonlinear terms in the FK equation and the coupling between species concentration and medium mass reduction.

To demonstrate the practical capabilities of the proposed model, we consider its application in the modeling of the onset of Alzheimer's disease. This particular illness stands as one of the predominant forms of dementia, accounting for approximately 60%-70% of its cases [19]. Alzheimer's disease is characterized by the agglomeration of protein fragments, specifically β -amyloid, forming extracellular deposits called neuritic plaques, the central core of which contains β -amyloid, while the surrounding corona contains degenerating neurons, primarily axons [55], and twisted strands of τ -protein, leading to intraneuronal neurofibrillary tangles, which consist in the abnormal accumulation of τ aggregates, forming filamentous structure within neurons [57, 20]. Observations indicate that the accumulation of this pathological material begins up to twenty years before the onset of the first symptoms of the disease [20, 21].

The remaining part of the paper is organized as follows. In Section 2, we introduce the mathematical model. In Section 3, we outline the most important features of the DG method for space discretization and introduce useful definitions necessary to our analysis. In Section 4, we derive the semi-discrete formulation of our problem by applying the DG discretization on space. In Section 5 we introduce the discretization in time and the two possible treatments of the nonlinear terms. In Section 6, we verify the validity of the numerical model through a convergence test performed on a system of decoupled equations and we also verify its robustness in the case of coupled equations with a simulation on three-dimensional domains. In Section 7, we present simulations performed applying our model to the atrophy of the brain induced by Alzheimer's disease. To do so, we consider the case in which we assume the atrophy to be an infinite process. In Section 8, we present our conclusions, a possible extension of our work to the case of finite deformation applying a nonlinear elasticity equation, and discuss future developments.

2. Multiphysics coupled model of tissue atrophy and biological agent diffusion

In this section, we introduce a multiphysics model to investigate tissue atrophy driven by the spread of a biological agent, with a focus on applications to Alzheimer's disease. The novelty of the model relies on a new constitutive equation for the inelastic component of the stress tensor used to model tissue atrophy. This method, based on the usage of polytopal elements, facilitates the discretization of complex domains. Specifically, we adopt the FK equation to

model the spreading of the species concentration. Tissue atrophy is characterized through a morpho-elastic framework, which combines the effects of mass loss and tissue elasticity to determine the resulting tissue morphology, employing a multiplicative decomposition of the deformation gradient into an elastic and a growth-related component [12], where the latter depends on the evolution of tissue loss [41, 53]. The model connects the morpho-elastic response to the agent concentration by defining an evolution law for inelastic strain, regulated by the concentration of the agent through a logistic-type differential equation. The strong formulation of the coupled model reads

$$\left\{ \begin{array}{ll} J \frac{\partial c}{\partial t} = \nabla_X \cdot (J\mathbf{F}^{-1}\mathbf{D}\mathbf{F}^{-T}\nabla_X c) + \alpha Jc(1-c) & \text{in } \Omega \times (0, T], \\ \dot{g} = \frac{1}{\tau}(g+1) \left(1 - \frac{1}{\beta}(g+1) \right) & \text{in } \Omega \times (0, T], \\ -\nabla_X \cdot \mathbf{P} = \mathbf{0} & \text{in } \Omega \times (0, T], \\ (J\mathbf{F}^{-1}\mathbf{D}\mathbf{F}^{-T}\nabla_X c) \cdot \mathbf{n} = 0 & \text{on } \partial\Omega \times (0, T], \\ \mathbf{P}(\mathbf{u})\mathbf{n} = \mathbf{0} & \text{on } \Gamma_N^{\mathbf{u}} \times (0, T], \\ \mathbf{u} = \mathbf{u}_D & \text{on } \Gamma_D^{\mathbf{u}} \times (0, T], \\ c(\mathbf{x}, 0) = c_0 & \text{in } \Omega, \\ g(\mathbf{x}, 0) = g_0 & \text{in } \Omega, \end{array} \right. \quad (1)$$

and is derived as follows.

2.1. Modeling the biological agent dynamics

We characterize the spreading of the agent by the FK equation [38, 49], which is frequently used in literature to model the propagation of a favored gene in population dynamics, as it serves as the simplest reaction-diffusion equation that incorporates two critical effects: dispersion (diffusive term) and proliferation (reactive term) [47], [44]. We introduce the relative concentration of the agent as $c = c(\mathbf{x}, t) : \Omega_t \times [0, T] \rightarrow \mathbb{R}$. The FK equation for the relative concentration $c = c(\mathbf{x}, t)$ can be formulated as follows:

$$\left\{ \begin{array}{ll} \frac{\partial c}{\partial t} = \nabla \cdot (\mathbf{D}\nabla c) + \alpha c(1-c) & \text{in } \Omega_t \times (0, T], \\ (\mathbf{D}\nabla c) \cdot \mathbf{n} = 0 & \text{on } \partial\Omega \times (0, T], \\ c(\mathbf{x}, 0) = c_0(\mathbf{x}) & \text{in } \Omega_t. \end{array} \right. \quad (2)$$

Here \mathbf{n} is the normal unit vector to the Neumann boundary, and $c_0(\mathbf{x})$ is the initial condition, which gives us the value and distribution of the concentration of the agent at the initial time $t = 0$. The diffusion tensor $\mathbf{D}(\mathbf{x})$ describes the directions and velocity of the agent spreading in the tissue. We assume the diffusion tensor to be symmetric and positive definite. In equation (2), $\alpha = \alpha(\mathbf{x})$ is the reaction coefficient, modeling misfolding, clearance, and aggregation of the biological agents.

Appropriate boundary conditions complement the FK equation. Specifically, we impose a homogeneous Neumann boundary condition that indicates the absence of flux of the agents across the boundary.

Remark 1. For all $\mathbf{x} \in \Omega_t, t \in [0, T], 0 \leq c_0(\mathbf{x}) \leq 1$ and $c_0(\mathbf{x}) \in H^1(\Omega_t)$ and taking homogeneous Neumann boundary conditions on the all boundary $\partial\Omega_t$, it is possible to prove that there exists a unique solution of (2) such that $0 \leq c(\mathbf{x}, t) \leq 1 \forall \mathbf{x} \in \Omega, \forall t > 0$ a.e.. In particular this means that, starting from a positive concentration, the solution propagates towards a stable equilibrium $c(\mathbf{x}, t) = 1$ with $t \rightarrow +\infty$ [17].

Since we will consider an atrophy process we will consider a reference configuration Ω , a current configuration Ω_t and a deformation ϕ . In particular, equation (2) is written in the current configuration Ω_t . However, when considering finite deformations, we need to solve (2) in the reference configuration Ω . Then, the FK equation can be rewritten in a Lagrangian setting as

$$\left\{ \begin{array}{ll} J \frac{\partial c}{\partial t} = \nabla_X \cdot (J\mathbf{F}^{-1}\mathbf{D}\mathbf{F}^{-T}\nabla_X c) + \alpha Jc(1-c), & \text{in } \Omega \times (0, T] \\ c(\mathbf{X}, 0) = c_0(\mathbf{X}), & \text{in } \Omega \\ J\mathbf{F}^{-1}\mathbf{D}\mathbf{F}^{-T}\nabla_X c \cdot \mathbf{n} = 0, & \text{on } \partial\Omega \times (0, T] \end{array} \right. \quad (3)$$

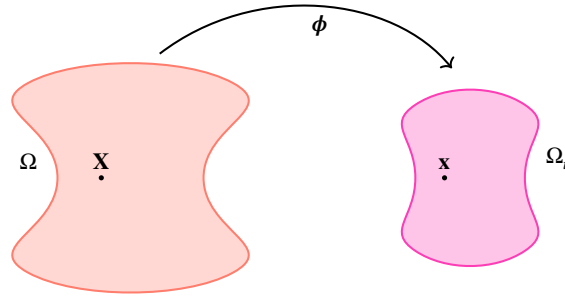


Figure 1: Graphic scheme of the reference domain Ω and the current domain Ω_t with the deformation ϕ .

where \mathbf{F} is the deformation gradient, J is the determinant of the deformation gradient and $\nabla_{\mathbf{X}}$ the gradient operator in the reference system of coordinates \mathbf{X} . The complete derivation of (3) can be found in Appendix A, while the definition of Ω , Ω_t and \mathbf{F} will be introduced in the following section (2.2).

2.2. Morpho-elasticity of tissue atrophy

In this section, we introduce the morpho-elastic model for tissue atrophy, assuming that the size of the tissue undergoing a pathological loss of mass is much larger than the characteristic size of a cell. Therefore, we describe the tissue as a continuum elastic body, where an active mass modulation induces the deformation.

We assume that the tissue occupies a domain $\Omega \subset \mathbb{R}^d$ at $t = 0$, which is assumed as the reference configuration, with $d = 2, 3$. The function that maps the reference domain to the current configuration Ω_t at time t is the deformation $\phi : \Omega \times (0, T] \rightarrow \mathbb{R}^d$. We also introduce the displacement field \mathbf{u} , defined as the function $\mathbf{u}(t, \mathbf{X}) = \phi(t, \mathbf{X}) - \mathbf{X}$. By $\mathbf{X} \in \Omega$, we indicate the generic point in the reference configuration. In contrast, we indicate with \mathbf{x} the corresponding point in the current configuration at time t so that $\mathbf{x} = \phi(\mathbf{X}, t)$. The deformation of the body can be described through the deformation gradient $\mathbf{F} = \nabla_{\mathbf{X}}\phi$, where $\nabla_{\mathbf{X}}$ denotes the gradient operator with respect to the referential coordinates.

To model the mass reduction, we exploit the framework of morpho-elasticity [12]. We consider a multiplicative decomposition of the deformation gradient [5] so that

$$\mathbf{F} = \mathbf{F}_e \mathbf{G}, \quad (4)$$

where \mathbf{F}_e represents the local elastic distortion of the material, while \mathbf{G} describes the local inelastic distortion due to the growth or atrophy of the elastic body. We next describe the mechanics of tissue atrophy and discuss the constitutive assumptions. Usually, mass loss takes place on a much longer time scale than the elastic deformations' time scale. Therefore, we can assume quasi-static deformations and neglect inertial effects. Hence, the balance of the linear momentum reads

$$\begin{cases} -\nabla_{\mathbf{X}} \cdot \mathbf{P} = \mathbf{0} & \text{in } \Omega \times (0, T], \\ \mathbf{P}(\mathbf{u})\mathbf{n} = \mathbf{0} & \text{on } \Gamma_N^{\mathbf{u}} \times (0, T], \\ \mathbf{u} = \mathbf{u}_D & \text{on } \Gamma_D^{\mathbf{u}} \times (0, T]. \end{cases} \quad (5)$$

where \mathbf{P} is the first Piola-Kirchhoff stress tensor, $\nabla_{\mathbf{X}} \cdot$ is the divergence operator in the reference configuration. Additionally, we define $\Gamma_N^{\mathbf{u}}$ as the Neumann boundary region where we assume we have no traction (i.e. homogeneous Neumann boundary conditions), while $\Gamma_D^{\mathbf{u}}$ represents the portion of the boundary where we impose Dirichlet boundary conditions \mathbf{u}_D , needed to block rigid motion. As usual, we assume $\Gamma_D^{\mathbf{u}} \cup \Gamma_N^{\mathbf{u}} = \partial\Omega$ and $\Gamma_D^{\mathbf{u}} \cap \Gamma_N^{\mathbf{u}} = \emptyset$.

In what follows, we describe the tissue as a hyperelastic material, i.e. we postulate the existence of a strain energy density $\Psi(\mathbf{X}, \mathbf{F})$. We will omit the explicit dependence on \mathbf{X} and \mathbf{F} whenever convenient. Standard thermodynamic arguments [4] allows us to write

$$\mathbf{P} = \frac{\partial \Psi}{\partial \mathbf{F}}.$$

By following the standard theory of morpho-elasticity [5, 12], the strain energy density $\Psi(\mathbf{X}, \mathbf{F})$ of the material can be written as

$$\Psi(\mathbf{X}, \mathbf{F}, t) = (\det \mathbf{G}(\mathbf{X}, t)) \Psi_0(\mathbf{F}\mathbf{G}^{-1}(\mathbf{X}, t)),$$

where $\Psi_0(\mathbf{F}_e)$ represents the strain energy density of the material in its relaxed state, i.e. the stress vanishes if there is no elastic distortion, so that

$$\left. \frac{\partial \Psi_0}{\partial \mathbf{F}_e} \right|_{\mathbf{F}_e=\mathbf{I}} = \mathbf{0}. \quad (6)$$

In this work we will assume to have an isotropic mass loss, i.e.

$$\mathbf{G} = (1 + g)\mathbf{I}. \quad (7)$$

The expression of the Piola-Kirchhoff stress tensor becomes

$$\mathbf{P} = \det(\mathbf{G}) \frac{\partial \Psi_0}{\partial \mathbf{F}_e} \mathbf{G}^{-T}. \quad (8)$$

In the following paragraph we present the theoretical framework of the case of small deformations.

2.2.1. Evolution law for the inelastic tensor \mathbf{G}

The evolution law for the inelastic tensor \mathbf{G} introduced in equation (4) must be constitutively provided. We assume that the atrophy of the tissue is isotropic, with $\mathbf{G} = (1 + g)\mathbf{I}$. The scalar variable $g = g(\mathbf{X}, t)$ accounts for the local mass reduction triggered by the local concentration of the biological agent. Specifically, the mass density per unit reference volume at time t in the reference configuration is given by

$$\rho_t(\mathbf{X}, t) = \rho_0(\mathbf{X}) \det \mathbf{G}(\mathbf{X}, t),$$

where ρ_0 is the mass density per unit volume in the relaxed state. In this model, we assume that no mass change occurs if the agent's concentration $c(\mathbf{x}, t)$ is below a critical threshold c_{cr} . Tissue atrophy takes place when the concentration c is above such a critical threshold. To mimic this behavior, we introduce the following logistic-type equation for the evolution of $g(t)$

$$\begin{cases} \dot{g} = \frac{1}{\hat{\tau}}(1 + g) \left(1 - \frac{1 + g}{\beta} \right) & \text{in } (0, T], \\ g(\mathbf{x}, 0) = 0 & \text{in } \Omega, \end{cases} \quad (9)$$

where

$$\beta = \begin{cases} 1 & \text{if } c \leq c_{cr}, \\ 1 - \gamma \frac{c - c_{cr}}{1 - c_{cr}} & \text{if } c > c_{cr}. \end{cases} \quad (10)$$

The parameter $\hat{\tau}$ in equation (9) represents the characteristic time of tissue atrophy, and $\gamma \in (0, 1)$ is a parameter at our disposal, modeling the maximum atrophy induced by the pathology. Moreover, note that $1 - \gamma$ in equation (10) represents the minimal value of β , with β modeling the relative mass remained after the atrophy process. There are other possibilities to model the evolution of $g(t)$. For example, in [53], the authors proposed an linear atrophy law, however this leads to an exponential decay of tissue mass to zero. In contrast, the logistic equation proposed in our manuscript avoids this issue by introducing nonlinearity, ensuring that $g > -\gamma > -1$, i.e., the mass density does not approach zero as t increases.

Remark 2. (Stability analysis) We compute the equilibria of equation (9) by imposing the right-hand side of the equation equal to 0, and find $g + 1 = \{\beta, 0\}$. Now we observe that by evaluating the derivative $\frac{\partial \dot{g}}{\partial g}$ in $g = \beta - 1$ we obtain:

$$\left. \frac{1}{\hat{\tau}} \left(1 - \frac{2}{\beta}(1 + g) \right) \right|_{g=\beta-1} = -\frac{1}{\hat{\tau}} < 0,$$

which implies that $g = \beta - 1$ is a stable equilibrium for the logistic equation. Furthermore, we observe that, when $c \leq c_{cr}$, the stable equilibrium $g = \beta - 1 = 0$. In fact, we do not have atrophy caused by the biological agent. When, instead, $c > c_{cr}$, the stable equilibria become $g = \beta - 1 = -\gamma \frac{c - c_{cr}}{1 - c_{cr}}$, which varies with the increase of the concentration of the agent. In particular, when $c = 1$, $g = \beta - 1 = -\gamma$, meaning that γ represents the absolute value of the maximum shrinkage that we can obtain. Indeed, the choice of a logistic function to describe the dynamic of g allows us to introduce a natural bound to mass loss, $\beta - 1 < g < 1$, while for a simpler model, such as a linear mass reduction, we would have predicted that $g \rightarrow -1$, i.e. a complete mass loss over time, which is unphysical.

Now, coupling together equations (3), (9) and (5) we recover the strong formulation of the coupled problem (1).

Remark 3. Since $0 \leq |g| \leq \beta - 1 \leq |\gamma|$, then, for small values of γ we are in the small deformation regime, and therefore the linear (12) and non-linear (7) formulations are consistent, as expected.

2.3. Weak formulation

Now we derive the variational formulation of problem (1). To begin with, we introduce functional spaces tailored for the solutions of the equations. To address the solution of the parabolic differential FK equation, we define the spaces: $W = H^1(\Omega)$. Turning to the solution g of the ODE (9), we introduce the space $Q = H^1(\Omega)$. Additionally, for the solution of the elasticity equation (5), we define $\mathbf{V} = \mathbf{H}^1(\Omega, \mathbb{R}^d)$, and $\mathbf{V}_0 = \mathbf{H}_{\Gamma_D}^1(\Omega, \mathbb{R}^d) := \{\mathbf{v} \in \mathbf{H}^1(\Omega, \mathbb{R}^d) : \mathbf{v}|_{\Gamma_D} = 0\}$. Furthermore, we utilize the conventional definition of the $L^2(\Omega)$ scalar product, represented as $(\cdot, \cdot)_\Omega$ with the associated norm denoted by $\|\cdot\|_\Omega$. This definition extends componentwise for vector-valued and tensor-valued functions [16]. The weak formulation of the problem described in System (1) becomes:

$\forall t \in (0, T]$ find $c(\mathbf{x}, t) \in W$, $g(\mathbf{x}, t) \in Q$ and $\mathbf{u}(\mathbf{x}) \in \mathbf{V}_0$ such that:

$$\begin{cases} \left(\mathbf{J} \frac{\partial c(\mathbf{x}, t)}{\partial t}, w \right)_\Omega + a_c(c(\mathbf{x}, t), w) - r_L^c(c(\mathbf{x}, t), w) + r_N^c(c(\mathbf{x}, t), c(\mathbf{x}, t), w) = 0 & \forall w \in W, \\ (\dot{g}(\mathbf{x}, t), p)_\Omega = r_L^g(g, p) - r_N^g(g, g, p) + F_g(p) & \forall p \in Q, \\ a_E(\mathbf{u}, \mathbf{v}) = \mathbf{0} & \forall \mathbf{v} \in \mathbf{V}_0, \\ c(\mathbf{x}, 0) = c_0(\mathbf{x}) & \text{in } \Omega, \\ g(\mathbf{x}, 0) = 0 & \text{in } \Omega, \end{cases} \quad (11)$$

where:

$$\begin{aligned} a_c(c, w) &= (\mathbf{J}\mathbf{F}^{-1}\mathbf{D}\mathbf{F}^{-T}\nabla c, \nabla w)_\Omega, & r_L^c(c, w) &= (\mathbf{J}\alpha c, w)_\Omega, \\ r_N^c(v, c, w) &= (\mathbf{J}\alpha(vc), w)_\Omega, & r_L^g(g, p) &= \left(\frac{1}{\hat{\tau}} \left(1 - \frac{2}{\beta(c)} \right) g, p \right)_\Omega, \\ r_N^g(g, p, q) &= \left(\frac{1}{\hat{\tau}\beta(c)} gp, q \right)_\Omega, & F_g(p) &= \frac{1}{\hat{\tau}} \left(\left(1 - \frac{1}{\beta(c)} \right), p \right)_\Omega, \\ a_E(\mathbf{u}, \mathbf{v}) &= (\mathbf{P}(\mathbf{u}), \nabla_X \mathbf{v})_\Omega, \end{aligned}$$

For all $c, w, v \in W$, $g, p, q \in Q$ and $\mathbf{u}, \mathbf{v} \in \mathbf{V}$.

2.3.1. Linearization of the mechanics of tissue atrophy

Let ε be $\max_{\mathbf{X} \in \Omega} \max_{t \in (0, T]} \|\mathbf{u}(\mathbf{X}, t)\|$, being $\|\cdot\|$ the Euclidean norm. The vector field \mathbf{u}_1 is the normalized counterpart of \mathbf{u} , i.e. $\mathbf{u}(\mathbf{X}, t) = \varepsilon \mathbf{u}_1(\mathbf{X}, t)$, where ε is a real positive number assumed small. Therefore, we can take a series expansion of \mathbf{G} (7) in ε , assuming \mathbf{G} to be a small perturbation of the identity, i.e.

$$\mathbf{G} = \mathbf{I} + \varepsilon \mathbf{G}_1 + o(\varepsilon). \quad (12)$$

This definition of \mathbf{G} is aligned with (7), taking $\varepsilon \mathbf{G}_1 = g \mathbf{I}$. Using the expansion (12) of \mathbf{G} we obtain:

$$\det \mathbf{G} = \det(\mathbf{I} + \varepsilon \mathbf{G}_1 + o(\varepsilon)) = 1 + \varepsilon \operatorname{tr} \mathbf{G}_1 + o(\varepsilon^2),$$

A coupled mathematical and numerical model for protein spreading and tissue atrophy applied to Alzheimer's disease

$$\mathbf{G}^{-1} = \mathbf{I} - \varepsilon \mathbf{G}_1 + o(\varepsilon),$$

$$\mathbf{F}\mathbf{G}^{-1} = (\mathbf{I} + \varepsilon \nabla \mathbf{u}_1)(\mathbf{I} - \varepsilon \mathbf{G}_1) + o(\varepsilon) = \mathbf{I} + \varepsilon(\nabla \mathbf{u}_1 - \mathbf{G}_1) + o(\varepsilon).$$

Performing a Taylor expansion on (8), the Piola-Kirchhoff stress tensor can be approximated as:

$$\begin{aligned} \mathbf{P} &= (1 + \varepsilon \operatorname{tr} \mathbf{G}_1) \left(\underbrace{\frac{\partial \Psi_0}{\partial \mathbf{F}_e}}_{\mathbf{0}} \Big|_{\mathbf{F}_e=\mathbf{I}} + \underbrace{\frac{\partial^2 \Psi_0}{\partial \mathbf{F}_e \partial \mathbf{F}_e}}_{\mathbb{C}} \Big|_{\mathbf{F}_e=\mathbf{I}} : \varepsilon(\nabla \mathbf{u}_1 - \mathbf{G}_1) \right) (\mathbf{I} - \varepsilon \operatorname{tr} \mathbf{G}_1)^T + o(\varepsilon) = \\ &= \varepsilon \mathbb{C} : (\nabla \mathbf{u}_1 - \mathbf{G}_1) + o(\varepsilon) = \mathbb{C} : (\nabla \mathbf{u} - g \mathbf{I}) + o(\varepsilon) = \mathbb{C} : \mathbf{E}_e + o(\varepsilon) \end{aligned} \quad (13)$$

where the term of order 0 in ε vanishes because of (6) and \mathbb{C} represents the fourth-order elasticity tensor, with

$$C_{ijkl} = \frac{\partial^2 \Psi_0}{\partial F_{eij} \partial F_{ehk}} \Big|_{\mathbf{F}_e=\mathbf{I}}, \quad C_{ijhk} = C_{jihk} = C_{ijkh} = C_{hkij}.$$

In (13), we have neglect the remainder $o(\varepsilon)$ and we take $\mathbf{E}_e = \frac{\nabla \mathbf{u} - g \mathbf{I} + (\nabla \mathbf{u} - g \mathbf{I})^T}{2}$. For an isotropic material, it is well-known that $\mathbf{P} = \mathbb{C} : \mathbf{E}_e = 2\mu \mathbf{E}_e + \lambda(\operatorname{tr}(\mathbf{E}_e))\mathbf{I}$, which gives

$$\mathbf{P} = 2\mu \left(\frac{\nabla \mathbf{u} + \nabla \mathbf{u}^T}{2} \right) + \lambda \nabla \cdot \mathbf{u} \mathbf{I} - 2\mu \left(\frac{g \mathbf{I} + (g \mathbf{I})^T}{2} \right) - \lambda \operatorname{tr} \left(\frac{g \mathbf{I} + (g \mathbf{I})^T}{2} \right) \mathbf{I}.$$

Under this assumption the Piola-Kirchhoff tensor simplifies into

$$\mathbf{P} = 2\mu \left(\frac{\nabla \mathbf{u} + \nabla \mathbf{u}^T}{2} \right) + \lambda \nabla \cdot \mathbf{u} \mathbf{I} - (2\mu + d\lambda)g \mathbf{I}, \quad (14)$$

where d is the space dimension.

Defining $\mathbf{E}(\mathbf{u}) = \frac{1}{2}(\nabla \mathbf{u} + \nabla \mathbf{u}^T)$, the symmetric part of the gradient of the displacement, we can write the elasticity equation as:

$$\begin{aligned} -\nabla \cdot \mathbf{P} &= -2\nabla \cdot (\mu \mathbf{E}(\mathbf{u})) - \nabla \cdot (\lambda \nabla \cdot \mathbf{u} \mathbf{I}) + \nabla \cdot ((2\mu + d\lambda)g \mathbf{I}) \\ &= -2\nabla \cdot (\mu \mathbf{E}(\mathbf{u})) - \nabla(\lambda \nabla \cdot \mathbf{u}) + \nabla((2\mu + d\lambda)g) = \mathbf{f}_u. \end{aligned}$$

We remark that the local change of volume due to atrophy is given by $\det \mathbf{G}$. In the linear elastic setting introduced in this section we get $\det \mathbf{G} = 1 + \operatorname{tr} g \mathbf{I} + o(\varepsilon) = 1 + 3g + o(\varepsilon)$. Thus, $3g$ serves as an indicator of the local volume change.

In a linear deformation regime, we can neglect the difference between the current domain Ω_t and the reference domain Ω , therefore, we assume $\Omega \simeq \Omega_t$, $\partial\Omega \simeq \partial\Omega_t$. In what follows we will derive the DG numerical formulation of the model in the linearized case. Indeed, the majority of the test cases will be performed under the assumption of linear elasticity since we have small deformations, therefore the assumption is valid. While, for the test case in which we consider a nonlinear elasticity, we will implement continuous elements for the elasticity. The implementation of a numerical DG method for the non linear elasticity equation is under study and will be subject of future works.

3. Discontinuous Galerkin formulation

Let \mathcal{T}_h a partition of the domain Ω using polygonal or polyhedral elements $K \in \mathcal{T}_h$. Here, $|K|$ denotes the measure of each element, h_K represents the diameter of each element, and $h = \max_{K \in \mathcal{T}_h} h_K < 1$. The interfaces of each element are the $(d-1)$ -dimensional intersections of adjacent facets. We distinguish two cases:

- case $d = 3$, in which the interfaces are triangles, the set of which we denote by \mathcal{F}^h ;
- case $d = 2$, in which the interfaces are line segments, the set of which we denote by \mathcal{F}^h .

Specifically, the set of interfaces \mathcal{F}_h comprises the union of boundary faces \mathcal{F}_h^B , lying on the boundary, and all interior faces \mathcal{F}_h^I . We can further categorize the set of boundary faces \mathcal{F}_h^B into interfaces where Dirichlet conditions are applied, \mathcal{F}_h^D , and interfaces where Neumann boundary conditions are applied, \mathcal{F}_h^N . We also assume that \mathcal{F}_h is aligned with Γ_D and Γ_N , implying that any element in \mathcal{F}_h^B is contained within either Γ_D or Γ_N .

We introduce the trace operators on the interior faces \mathcal{F}_h^I . We also employ the notation q^+ and q^- to signify traces of functions on the face $F \in \mathcal{F}_h^I$, in common between the elements K^+ and K^- , respectively, for a generic function q . For a scalar-valued function q , a vector-valued function \mathbf{v} and a tensor-valued function $\boldsymbol{\tau}$ we define:

- Average operator: $\{\{q\}\} = \frac{1}{2}(q^+ + q^-)$, $\{\{\mathbf{v}\}\} = \frac{1}{2}(\mathbf{v}^+ + \mathbf{v}^-)$ and $\{\{\boldsymbol{\tau}\}\} = \frac{1}{2}(\boldsymbol{\tau}^+ + \boldsymbol{\tau}^-)$
- Jump operator: $[\![\cdot]\!]$ on $F \in \mathcal{F}_h^I$: $[\![q]\!] = q^+\mathbf{n}^+ + q^-\mathbf{n}^-$, which returns a vector quantity, $[\![\mathbf{v}]\!] = \mathbf{v}^+ \cdot \mathbf{n}^+ + \mathbf{v}^- \cdot \mathbf{n}^-$, which returns a scalar quantity and $[\![\boldsymbol{\tau}]\!] = \boldsymbol{\tau}^+\mathbf{n}^+ + \boldsymbol{\tau}^-\mathbf{n}^-$, which returns a vector quantity.
- Tensorial-jump operator: $[\![\![\mathbf{v}]\!]\!] = \frac{1}{2}(\mathbf{v}^+ \otimes \mathbf{n}^+ + \mathbf{n}^+ \otimes \mathbf{v}^+) + \frac{1}{2}(\mathbf{v}^- \otimes \mathbf{n}^- + \mathbf{n}^- \otimes \mathbf{v}^-)$, which returns a tensorial quantity.

On $F \in \mathcal{F}_h^D$, we set the following trace operators for the test functions as $\{\{q\}\} = q$, $\{\{\mathbf{v}\}\} = \mathbf{v}$, $\{\{\boldsymbol{\tau}\}\} = \boldsymbol{\tau}$ and $[\![\mathbf{v}]\!] = \frac{1}{2}(\mathbf{v} \otimes \mathbf{n} + \mathbf{n} \otimes \mathbf{v})$. Additionally, for the trial functions we define the traces operator on the faces of the Dirichlet boundary as $[\![p]\!] = (p - h_D)\mathbf{n}$, $[\![\mathbf{u}]\!] = (\mathbf{u} - \mathbf{h}_D) \cdot \mathbf{n}$, $[\![\boldsymbol{\tau}]\!] = (\boldsymbol{\tau} - \boldsymbol{\tau}_D)\mathbf{n}$ and $[\![\![\mathbf{v}]\!]\!] = \frac{1}{2}((\mathbf{v} - \mathbf{h}_D) \otimes \mathbf{n} + \mathbf{n} \otimes (\mathbf{v} - \mathbf{h}_D))$, with \otimes defined as $\mathbf{a} \otimes \mathbf{b} := \mathbf{a}\mathbf{b}^T$ meaning $(\mathbf{a} \otimes \mathbf{b})_{ij} := a_i b_j \mathbf{e}_i \otimes \mathbf{e}_j$, and h_D , \mathbf{h}_D and $\boldsymbol{\tau}_D$ are the Dirichlet boundary conditions of h , \mathbf{h} and $\boldsymbol{\tau}$, respectively. The average and jump operators are essential to ensure the communication of the solution between neighboring elements [65]. We refer the reader to Appendix (B) for the derivation of the DG formulation.

We define the penalty functions $\eta : \mathcal{F}_h \rightarrow \mathbb{R}$ and $\xi : \mathcal{F}_h \rightarrow \mathbb{R}_+$ defined face-wise as:

$$\eta = \begin{cases} \eta_0 \max\{\{d^K\}_H, \{\alpha\}_H\} \frac{p_c^2}{\{h_K\}_H}, & \text{on } F \in \mathcal{F}_h^I, \\ \eta_0 \max\{d^K, \alpha\} \frac{p_c^2}{h_K}, & \text{on } F \in \mathcal{F}_h^D, \end{cases} \quad \xi = \begin{cases} \xi_0 \{\tilde{\mathbf{C}}_E^K\}_H \frac{p_{\mathbf{u}}^2}{\{h_K\}_H}, & \text{on } F \in \mathcal{F}_h^I, \\ \xi_0 \tilde{\mathbf{C}}_E^K \frac{p_{\mathbf{u}}^2}{h_K}, & \text{on } F \in \mathcal{F}_h^D, \end{cases} \quad (15)$$

where $\{\cdot\}_H$ denotes the harmonic average operator on $F \in \mathcal{F}_h^I$, $\{h_K\}_H = 2h_{K^+}h_{K^-}/(h_{K^+} + h_{K^-})$, with h_{K^+} and h_{K^-} are the sizes of the neighboring elements K_+ and $K_- \in \mathcal{F}_h$ respectively [68]. In (15) η_0 and ξ_0 are constants chosen sufficiently large to guarantee the stability of the methods, d^K and $\tilde{\mathbf{C}}_E^K$ are the norms of the diffusion tensor $\tilde{\mathbf{D}} = \mathbf{F}^{-1}\mathbf{D}\mathbf{F}^{-T}$ and of the fourth-order elasticity tensor \mathbb{C} restricted on the element K . They are defined as $d^K := \|\sqrt{\tilde{\mathbf{D}}}\|_K$ and $\tilde{\mathbf{C}}_E^K := \|\sqrt{\mathbb{C}_E}\|_K$ for any $K \in \mathcal{T}_h$, α is the reaction coefficient of the FK equation, and p_c and $p_{\mathbf{u}}$ are the polynomial degree of the concentration and displacement solutions, respectively. The penalty functions appear in a stability term of the DG formulation, see Appendix (B), and they are used to ensure the continuity of the final solution.

We define: $W_h^{DG} := \{w \in L^2(\Omega) : w|_K \in \mathbb{P}_{p_c}(K) \forall K \in \mathcal{T}_h\}$, $Q_h^{DG} := \{q \in L^2(\Omega) : q|_K \in \mathbb{P}_{p_g}(K) \forall K \in \mathcal{T}_h\}$ and $\mathbf{V}_h^{DG} := \{\mathbf{v} \in L^2(\Omega; \mathbb{R}^d) : \mathbf{v}|_K \in [\mathbb{P}_{p_{\mathbf{u}}}(K)]^d \forall K \in \mathcal{T}_h\}$, where the space $\mathbb{P}_{p_*}(K)$ is the space of the piecewise polynomials of degree p_* in the mesh element K , for $*$ = c, g, \mathbf{u} .

4. DG semi-discrete formulation

In this section we present the DG semi-discrete formulation of the weak problem (11), an example of a more detailed derivation for the FK equation can be found in Appendix B. Setting $\int_{\mathcal{F}_h} = \sum_{F \in \mathcal{F}_h} \int_F$, we define the following bilinear forms:

A coupled mathematical and numerical model for protein spreading and tissue atrophy applied to Alzheimer's disease

- $\mathcal{A}_c : W_h^{DG} \times W_h^{DG} \rightarrow \mathbb{R}$:

$$\begin{aligned} \mathcal{A}_c(c_h, w_h) &:= \int_{\Omega} \mathbf{JF}^{-1} \mathbf{DF}^{-T} \nabla_h c_h \cdot \nabla_h w_h \, d\mathbf{X} + \int_{\mathcal{F}_h^I \cup \mathcal{F}_h^D} \eta \llbracket c_h \rrbracket \cdot \llbracket w_h \rrbracket \, dS \\ &\quad - \int_{\mathcal{F}_h^I \cup \mathcal{F}_h^D} (\llbracket \mathbf{JF}^{-1} \mathbf{DF}^{-T} \nabla_h c \rrbracket \cdot \llbracket w_h \rrbracket + \llbracket c_h \rrbracket \cdot \llbracket \mathbf{JF}^{-1} \mathbf{DF}^{-T} \nabla_h w_h \rrbracket) \, dS \quad \forall c_h, w_h \in W_h^{DG} \end{aligned}$$

- $\mathcal{A}_E : \mathbf{V}_h^{DG} \times \mathbf{V}_h^{DG} \rightarrow \mathbb{R}$:

$$\begin{aligned} \mathcal{A}_E(\mathbf{u}_h, \mathbf{v}_h) &:= \int_{\Omega} (2\mu \boldsymbol{\varepsilon}(\mathbf{u}_h) : \boldsymbol{\varepsilon}(\mathbf{v}_h) + \lambda \nabla_h \cdot \mathbf{u}_h \nabla_h \cdot \mathbf{v}_h) \, d\mathbf{X} + \int_{\mathcal{F}_h^I \cup \mathcal{F}_h^D} \xi \llbracket \mathbf{u}_h \rrbracket : \llbracket \mathbf{v}_h \rrbracket \, dS \\ &\quad - \int_{\mathcal{F}_h^I \cup \mathcal{F}_h^D} (\llbracket 2\mu \boldsymbol{\varepsilon}(\mathbf{u}_h) + \lambda \nabla_h \cdot \mathbf{u}_h \rrbracket : \llbracket \mathbf{v}_h \rrbracket + \llbracket \mathbf{u}_h \rrbracket : \llbracket 2\mu \boldsymbol{\varepsilon}(\mathbf{v}_h) + \lambda \nabla_h \cdot \mathbf{v}_h \rrbracket) \, dS \quad \forall \mathbf{u}_h, \mathbf{v}_h \in \mathbf{V}_h^{DG}, \end{aligned}$$

- $\mathcal{B}_E : Q_h^{DG} \times \mathbf{V}_h^{DG} \rightarrow \mathbb{R}$:

$$\mathcal{B}_E(p_h, \mathbf{v}_h) = \int_{\Omega} (2\mu + d\lambda) p_h \nabla_h \cdot \mathbf{v}_h \, d\mathbf{X} - \int_{\mathcal{F}_h^I \cup \mathcal{F}_h^D} (2\mu + d\lambda) \llbracket p_h \mathbf{I} \rrbracket : \llbracket \mathbf{v}_h \rrbracket \, dS \quad \forall p_h \in Q_h^{DG}, \mathbf{v}_h \in \mathbf{V}_h^{DG}.$$

In the above definitions, ∇_h denotes the elementwise gradient [18]. Employing the aforementioned bilinear forms, we derive the semi-discrete formulation of model (11) as follows:

For any $t \in (0, T]$ find $c_h(t) \in W_h^{DG}$, $g_h(t) \in Q_h^{DG}$ and $\mathbf{u}_h(t) \in \mathbf{V}_h^{DG}$ such that:

$$\begin{cases} (J\dot{c}_h, w_h)_{\Omega} + \mathcal{A}_c(c_h, w_h) - r_L(c_h, w_h) + r_N(c_h, c_h, w_h) = \mathbf{0} & \forall w_h \in W_h^{DG}, \\ (\dot{g}_h, p_h)_{\Omega} = r_L^g(g_h, p_h) - r_N^g(g_h, g_h, p_h) + F_g(p_h) & \forall p_h \in Q_h^{DG}, \\ \mathcal{A}_E(\mathbf{u}_h, \mathbf{v}_h) - \mathcal{B}_E(g_h, \mathbf{v}_h) = \mathbf{0} & \forall \mathbf{v}_h \in \mathbf{V}_h^{DG}, \\ c_h(0) = c_{0h}, \quad g_h(0) = 0 & \text{in } \Omega_h. \end{cases} \quad (16)$$

In Equation (16), c_{0h} is a suitable approximation of the initial conditions c_0 in the discrete space W_h^{DG} .

4.1. Algebraic formulation

Let $\{\phi_j\}_{j=1}^{N_c}$, $\{q_j\}_{j=1}^{N_g}$, and $\{\psi_j\}_{j=1}^{N_u}$ be suitable basis functions for the discrete spaces W_h^{DG} , Q_h^{DG} , and \mathbf{V}_h^{DG} , respectively. Then we can write:

$$c_h(\mathbf{x}, t) = \sum_{j=1}^{N_c} C_n(t) \phi_j(\mathbf{x}), \quad g_h(\mathbf{x}, t) = \sum_{j=1}^{N_g} g_n(t) q_j(\mathbf{x}), \quad \mathbf{u}_h(\mathbf{x}, t) = \sum_{j=1}^{N_u} U_n(t) \psi_j(\mathbf{x}).$$

Many different choices of the basis functions can be adopted; however, in this work, we focus on classical Lagrange basis functions [18, 58]. We denote by $\mathbf{C} := [C_n]_{n=1}^{N_c} \in \mathbb{R}^{N_c}$, $\mathbf{g} := [G_n]_{n=1}^{N_g} \in \mathbb{R}^{N_g}$ and $\mathbf{U} := [U_n]_{n=1}^{N_u} \in \mathbb{R}^{dN_u}$ the vector of the expansion coefficients and we define the following matrices: for $i, j = 1, \dots, N_c$:

$$\begin{aligned} [\mathbf{M}_c]_{ij} &= (\phi_j, \phi_i)_{\Omega} && \text{(Mass matrix);} \\ [\mathbf{A}_c]_{ij} &= \mathcal{A}_c(\phi_j, \phi_i) && \text{(Stiffness matrix);} \\ [\mathbf{M}_\alpha]_{ij} &= (\alpha \phi_j, \phi_i)_{\Omega} && \text{(Linear reaction matrix);} \\ [\tilde{\mathbf{M}}_\alpha(\mathbf{C}(t))]_{ij} &= (\alpha c_h(t) \phi_j, \phi_i)_{\Omega} && \text{(Nonlinear reaction matrix);} \end{aligned}$$

We also define for $i, j = 1, \dots, N_g$:

$$\begin{aligned} [\mathbf{M}_g]_{ij} &= (q_j, q_i)_\Omega && (g \text{ -mass matrix}); \\ [\mathbf{M}_\beta]_{ij} &= r_L^g(q_j, q_i) && (\text{Linear term matrix}); \\ [\tilde{\mathbf{M}}_\beta(\mathbf{g}(t))]_{ij} &= r_N^g(q_j, g_h(t), q_i) && (\text{Nonlinear term matrix}); \end{aligned}$$

and finally set, for $i, j = 1, \dots, N_u$:

$$\begin{aligned} [\mathbf{M}_E]_{ij} &= (\boldsymbol{\psi}_j, \boldsymbol{\psi}_i)_\Omega && (\text{Elasticity mass matrix}); \\ [\mathbf{K}_E]_{ij} &= \mathcal{A}_E(\boldsymbol{\psi}_j, \boldsymbol{\psi}_i) && (\text{Elasticity stiffness matrix}); \\ [\mathbf{B}_g]_{ij} &= \mathcal{B}_E(q_j, \boldsymbol{\psi}_i) && (g \text{ - displacement coupling matrix}). \end{aligned}$$

Moreover we define the forcing term $\mathbf{F}_g = [F_g(q_j)]_{j=1}^{N_g}$.

The algebraic form of (16) can be written as: Find $\mathbf{C}(t) \in \mathbb{R}^{N_c}$, $\mathbf{g}(t) \in \mathbb{R}^{N_g}$ and $\mathbf{U} \in \mathbb{R}^{d_{N_u}}$ such that $\forall t \in (0, T]$ we have:

$$\left\{ \begin{array}{l} \mathbf{M}_c \dot{\mathbf{C}}(t) + \mathbf{A}_c \mathbf{C}(t) - \mathbf{M}_\alpha \mathbf{C}(t) + \tilde{\mathbf{M}}_\alpha(\mathbf{C}(t)) \mathbf{C}(t) = \mathbf{0}, \quad t \in (0, T], \\ \mathbf{M}_g \dot{\mathbf{g}}(t) = \mathbf{M}_g \mathbf{g}(t) - \tilde{\mathbf{M}}_g(\mathbf{g}(t)) \mathbf{g}(t) + \mathbf{F}_g \quad t \in (0, T], \\ \mathbf{K}_E \mathbf{U} - \mathbf{B}_g^T \mathbf{g} = \mathbf{0}, \\ \mathbf{C}(0) = \mathbf{C}_0, \\ \mathbf{g}(0) = \mathbf{g}_0. \end{array} \right. \quad (17)$$

5. Fully discrete formulation

Now, let us present the fully discrete approximation of Equation (1). We apply the Crank-Nicolson method to discretize temporal derivatives, and we consider a semi-implicit treatment of the nonlinear terms, ultimately outlining the complete discrete formulation of our problem. To discretize the time evolution of (17) we define a partition of the time interval $[0, T]$ into N intervals: $0 = t_0 < t_1 < \dots < t_N = T$ and we assume a time step $\Delta t = t_{n+1} - t_n$, $n = 0, \dots, N - 1$. Consequently, the fully discrete formulation of Problem (1) becomes: Given $\mathbf{C}(0) = \mathbf{C}_0$ and $\mathbf{g}(0) = \mathbf{g}_0$, find $\mathbf{C}^{n+1} \simeq \mathbf{C}(t_{n+1})$, $\mathbf{g}^{n+1} \simeq \mathbf{g}(t_{n+1})$ and $\mathbf{U}^{n+1} \simeq \mathbf{U}(t_{n+1}) \in \mathbb{R}^{d_{N_u}}$ for $n = 1, \dots, N - 1$:

$$\left\{ \begin{array}{l} \mathbf{M}_c \mathbf{C}^{n+1} + \frac{\Delta t}{2} (\mathbf{A}_c - \mathbf{M}_\alpha + \tilde{\mathbf{M}}_\alpha(\mathbf{C}^*)) \mathbf{C}^{n+1} = \mathbf{M}_c \mathbf{C}^n - \frac{\Delta t}{2} (\mathbf{A}_c - \mathbf{M}_\alpha + \tilde{\mathbf{M}}_\alpha(\mathbf{C}^*)) \mathbf{C}^n, \\ \mathbf{M}_g \mathbf{g}^{n+1} + \frac{\Delta t}{2} (\tilde{\mathbf{M}}_\beta(\mathbf{g}^*) - \mathbf{M}_\beta) \mathbf{g}^{n+1} = \mathbf{M}_g \mathbf{g}^n + \frac{\Delta t}{2} (\mathbf{M}_\beta - \tilde{\mathbf{M}}_\beta(\mathbf{g}^*)) \mathbf{g}^n + \frac{\Delta t}{2} (\mathbf{F}_g^{n+1} + \mathbf{F}_g^n), \\ \mathbf{K}_E \mathbf{U}^{n+1} - \mathbf{B}_g^T \mathbf{g}^{n+1} = \mathbf{0}, \end{array} \right.$$

where $\mathbf{C}^* = \frac{3}{2} \mathbf{C}^n - \frac{1}{2} \mathbf{C}^{n-1}$ and $\mathbf{g}^* = \frac{3}{2} \mathbf{g}^n - \frac{1}{2} \mathbf{g}^{n-1}$ are a second-order linear extrapolation of the solution at time t_{n+1} . This choice provides a semi-implicit approach that is linear at each time step. For the FK equation, this treatment of nonlinearity guarantees good accuracy without needing a nonlinear iterative solver [6].

In Algorithm 1, we summarize the basic idea of the complete numerical solver. In particular, due to the coupling strategy at the basis of the mathematical model, it is possible to construct an efficient staggered approach for time integration. In particular, at any time t_n , it can be solved the FK equation first, using the deformation tensor \mathbf{F} computed at the previous timestep t_{n-1} . Then the updated value c_h^n is used to derive g_h^n , which is then used in the elasticity problem solver to derive \mathbf{u}_h^n .

6. Numerical results

In this section, we present the results of a numerical convergence test on a system of decoupled equations conducted to demonstrate the accuracy of the proposed method, and of simulations on a three-dimensional spherical domain aimed

Algorithm 1 Numerical algorithm summarizing the basic steps of the numerical scheme. We report the references to the problem in its strong formulation.

Input: c_{h0} and g_{h0}
while $t_n \leq T$ **do**
 Solve FK $\rightarrow c_h^n$ (2)
 if $c_h^n < c_{cr}$ **then**
 $\beta \leftarrow 1$
 else
 $\beta \leftarrow \beta(c_h^n)$
 end if
 Solve Logistic Law with parameter $\beta \rightarrow g_h^n$ (9)
 Use g_h^n to define the growth tensor and $\mathbf{P}(\mathbf{u}_h^n)$ (14)
 Solve Elasticity Equation $\rightarrow \mathbf{u}_h^n$ (5)
 $t_n \rightarrow t_{n+1}$
end while

Table 1

Parameters used in the test cases 1 and 2. These values have been found in the literature and the references are reported in the table.

Parameters	Values	Reference	Parameters	Values	Reference
d	8.00 [mm ² /year]	[9]	λ	505 [Pa]	[7]
α	0.90 [1/years]	[9]	μ	216 [Pa]	[7]
γ	0.05 [-]		$\hat{\tau}$	1 [year]	

to verify the robustness of the method with coupled equations. The numerical simulations are done using the FEniCS finite element software [11]. This software allows us to perform numerical simulations on a 3-dimensional domain with a mesh of tetrahedral elements.

From an algebraic point of view, we use the MUMPS solver to solve the FK and the logistic equation. Indeed, MUMPS is a parallel direct solver [56] that allows solving the system with a high level of accuracy and efficiency. In contrast, due to the large dimension of the elasticity problem whose solution is vectorial, a direct solver would be inefficient; for this reason, we employ the iterative solver GMRES with a SOR preconditioner for the elasticity equation.

To perform a convergence test we denote the L^2 norm as $\|\cdot\|_{L^2}$ on Ω , and the L^2 -norm on a set of faces \mathcal{F} $\|\cdot\|_{\mathcal{F}}^2 := \sum_{F \in \mathcal{F}} \|\cdot\|_{L^2(F)}^2$. In the convergence test, we also evaluate the errors in DG-norm, defined as:

$$\|c\|_{DG} = \|\sqrt{J\mathbf{F}^{-1}\mathbf{D}\mathbf{F}^{-T}}\nabla_h c\| + \|\sqrt{\eta}\llbracket c \rrbracket\|_{\mathcal{F}_h^I \cup \mathcal{F}_h^D} \quad \forall c \in H^1(\mathcal{F}_h),$$

$$\|\mathbf{u}\|_{DG} = \|\sqrt{C_E}[\varepsilon_h(\mathbf{u})]\| + \|\sqrt{\xi}\llbracket \mathbf{u} \rrbracket\|_{\mathcal{F}_h^I \cup \mathcal{F}_h^D} \quad \forall \mathbf{u} \in \mathbf{H}^1(\mathcal{F}_h, \mathbb{R}^d),$$

where we consider $\mathbf{F} = \mathbf{I}$ and $J = \det(\mathbf{F}) = 1$ if we are in the linear elasticity framework. The DG-norm is the sum of the H^1 -seminorm and the norm of jumps on the mesh faces. This is required in the error analysis of discontinuous Galerkin formulations. For details on the topic, we refer to [65].

6.1. Test case 1: convergence analysis of a three-dimensional test case

In this test case, we perform a convergence analysis employing a manufactured exact solution considering the simplified framework of linear elasticity. For this reason, we need to introduce forcing terms both for the FK equation and for the elasticity equation, which will be disregarded for the other numerical test cases, as they don't appear in the model. We will also employ the parameters shown in Table 1. Notice that this set of parameters is consistent with the forthcoming application of Section (7) [6, 7].

We consider a cubic domain $\Omega = (0 \text{ m}, 1 \text{ m})^3$ and a time interval $[0, 0.1]$ [years] with a time step $\Delta t = 10^{-3}$ [years]. We impose as exact solution, the following manufactured solution:

$$c(\mathbf{X}, t) = (\cos(\pi X)\cos(\pi Y)\cos(\pi Z) + 2)e^t, \quad g(\mathbf{X}, t) = 1.0/(2e^{t/\tau} - 1.0),$$

$$\mathbf{u}(\mathbf{X}) = \begin{bmatrix} -\cos(2\pi X)\cos(2\pi Y) \\ \sin(2\pi X)\sin(2\pi Y) \\ Z \end{bmatrix},$$

from which we have to derive suitable forcing terms f_c and \mathbf{f}_u , while we consider homogeneous Neumann boundary conditions for the concentration, and, for simplicity, Dirichlet boundary conditions for the elasticity equations, derived from the manufactured exact solution. Additionally we choose the diffusion tensor as $\mathbf{D} = d\mathbf{I}$. We also choose $\beta = 1$ for any $t \geq 0$. Due to this choice, since β is constant and does not depend on the concentration c , the three equations are naturally decoupled.

Figure 2 shows the computed errors in the L^2 and DG norms of the errors as functions of the mesh size $h = 0.8660, 0.4330, 0.2165, 0.1083$, in logarithmic scale. We can see how the error's norms follow the expected trend of h^{p_*+1} for the L^2 -norms and of h^{p_*} for the DG -norms as proven for the FK equation, and the linear elasticity equation, with $* = c, \mathbf{u}$ [6, 7].

6.2. Test Case 2: simulation of coupled system on an idealized spherical geometry

In this section, we present the results obtained for a holed spherical domain $\Omega = \{\mathbf{X} \in \mathbb{R}^3 : 0.05^2 \leq X^2 + Y^2 + Z^2 \leq 0.1^2\}$ in the framework of linear elasticity. We define the outer boundary as the Neumann's boundary $\Gamma_N := \{\mathbf{X} \in \mathbb{R}^3 : X^2 + Y^2 + Z^2 = 0.1^2\}$ and the inner boundary as the Dirichlet's boundary: $\Gamma_D := \{\mathbf{X} \in \mathbb{R}^3 : X^2 + Y^2 + Z^2 = 0.05^2\}$. The goal of the test case is to provide a verification of the coupled model solver in a simplified geometrical setting.

Again, we choose $\mathbf{D} = d\mathbf{I}$ and we employ the parameters presented in Table 1. As for the initial condition, $c_0(\mathbf{X})$, we assume the biological agent causing the atrophy is primarily concentrated in a small portion of the domain. Specifically, we use a Gaussian-type distribution to represent this initial state

$$c(\mathbf{X}, 0) = A \exp \left[-\frac{1}{2} \left(\frac{|\mathbf{X} - \mathbf{X}_0|}{0.05} \right)^2 \right],$$

where $A \simeq 0.4$ represents the amplitude, and the center \mathbf{X}_0 is chosen to be $(0.05, 0.05, 0.05)$. Finally we enforce homogeneous Neumann boundary conditions to avoid the spreading of the agent outside the domain. For the displacement we impose we impose homogeneous Neumann boundary conditions on Γ_N (the outer boundary), as we do not have any external stress, and homogeneous Dirichlet boundary conditions on Γ_D (inner boundary), to block the infinitesimal rigid displacement, see Figure 3. The solutions in Figure 4 are computed with mesh size $h = 0.094$, time interval $\Delta t = 0.05$ years, and polynomial degree $p_* = 3$, with $* = c, g, \mathbf{u}$. We show a section of the holed sphere where we can see the initial concentration distribution and its evolution. At final time $T = 15$ years, we can see how both the concentration and the length reduction rate g have reached their maximal value, $c_h(\mathbf{X}, T) = 1.0$ and, $|g_h(\mathbf{X}, T)| = \gamma = 0.05$, in agreement with what is expected from the model.

7. Simulations on a real brain geometry

In this section, we present the simulation by applying our model to the problem of the onset of brain atrophy induced by Alzheimer's disease. In the following, we assume that the brain undergoes only small deformations, therefore we are still in the linear elasticity framework. It is important to note that the brain is composed of extremely soft material, even compared to other biological soft tissues [2]. Although nonlinear elasticity might initially appear to be a more appropriate framework for modeling such soft tissues, in this case, the mechanical deformations primarily represent the atrophy induced by Alzheimer's disease. Throughout the disease, the brain's loses approximately 1%-2% of its volume per year for the entire brain [3]. Consequently, the resulting atrophy remains relatively small, even after a decade.

We perform our simulations on the real geometry of a brain constructed from the MRI images of project OASIS [43]. The segmentation of the brain geometrical structure is performed using Freesurfer [64] starting from the union

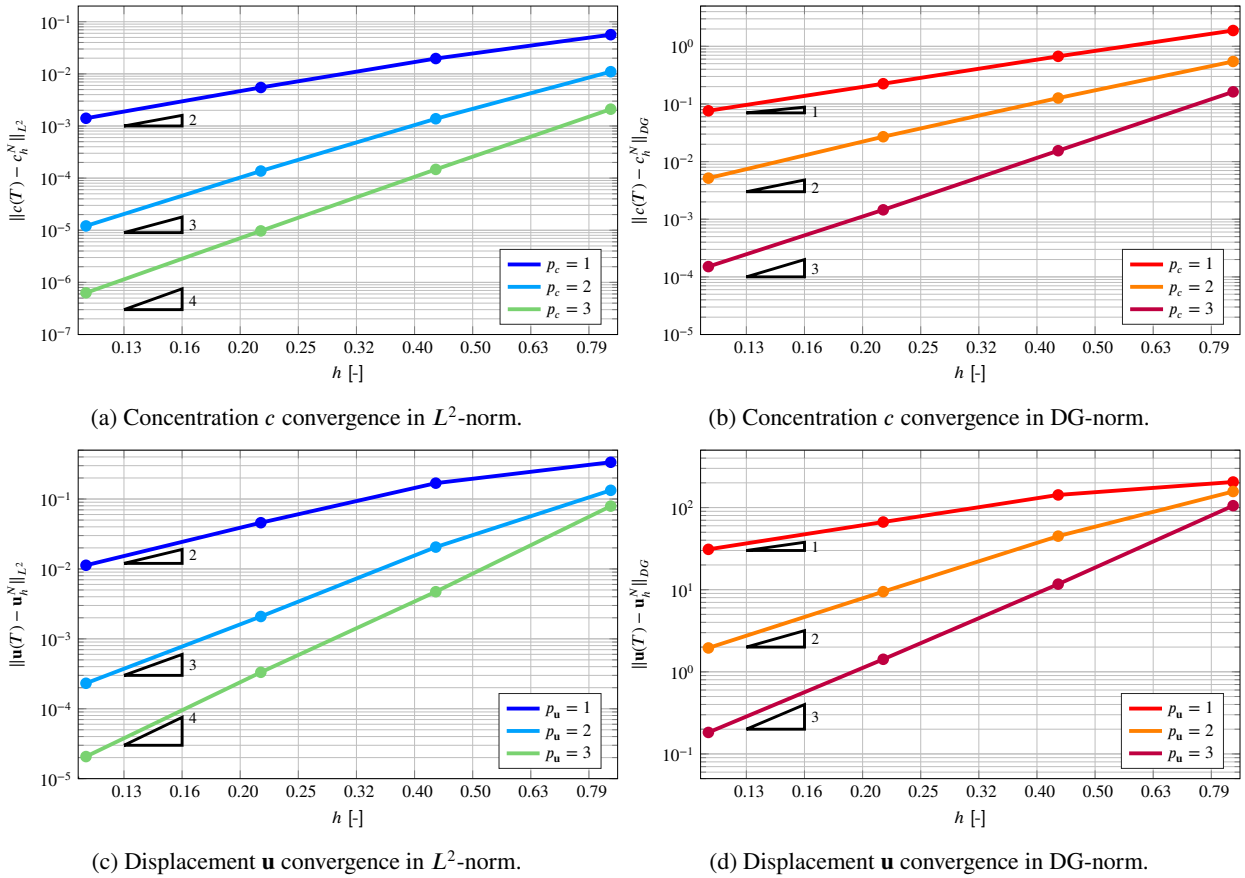


Figure 2: Test case 1: computed L^2 (left) and DG (right) errors as functions of the mesh-size h , with $h = 0.8660, 0.4330, 0.2165, 0.1083$ and polynomial degree of the basis functions p_c and $p_u = 1, 2, 3$, for the Test Case 1. The top panels show the results for the approximate concentration, while bottom panels show the results for the approximate displacement. All the errors are computed at final time $T = 0.1$ years. Logarithmic scales are used for all axes. The triangles indicate different convergence rates. The lines have been computed by interpolating the values of the error norms for each value of the mesh-size h .

Table 2

Parameters used in the test case of Section 7. The references associated with the reference values are reported in the table.

Parameters	Values	Reference	Parameters	Values	Reference
d_{ext}	8.00 [mm ² /year]	[9]	λ	2700 [Pa]	[51, 52]
d_{axn}	80.00 [mm ² /year]	[9]	μ	300 [Pa]	[51, 52]
α	0.90 [1/year]	[9]	$\hat{\tau}$	1 [year]	
γ	0.05 [-]				

of T1 weighted and T2 weighted MRI images. The construction of the final mesh, composed of 142 658 elements, is performed using the SVMTK library [60]. For this simulation, we consider a transversely isotropic diffusion tensor in the form $\mathbf{D} = d_{ext}\mathbf{I} + d_{axn}(\mathbf{n} \otimes \mathbf{n})$, where the versor \mathbf{n} locally represents the axonal directions inside the brain [9, 6]. The reconstruction of the axonal directions is performed from diffusion-weighted medical images by using Freesurfer and Nibabel [59] as explained in [60].

We impose homogeneous Neumann boundary conditions for the concentration on the whole boundary $\partial\Omega$. Concerning the displacement, we impose homogeneous Dirichlet conditions on the brain stem and homogeneous

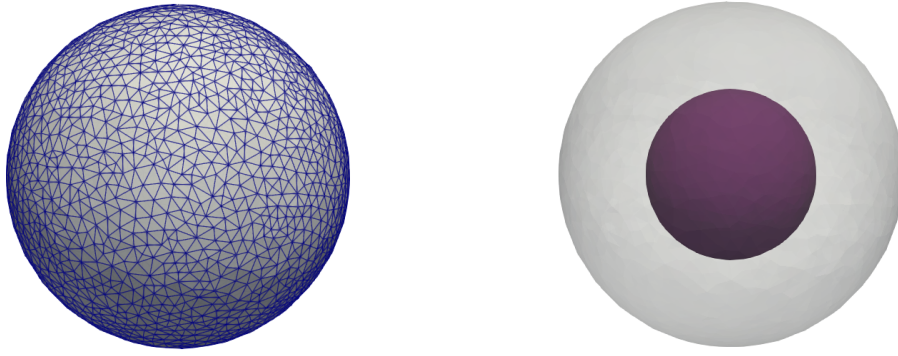


Figure 3: An external representation of the mesh (left) and a visualization of the ventricles boundary in purple and of the skull in transparency (right).

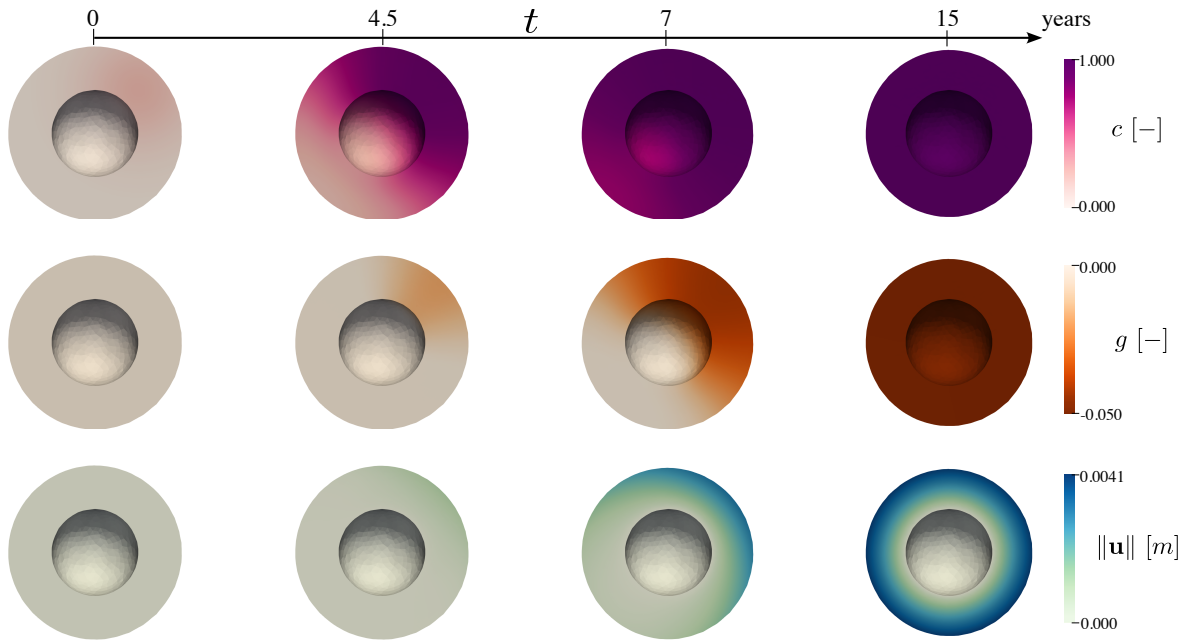


Figure 4: Test Case 2: concentration, atrophy rate, and norm of the displacement with $\hat{\tau} = 1$ year at time $t = 0, 4, 10, 15$ years, from left to right, obtained with polynomial degree $p_c = p_g = p_u = 3$.

Neumann conditions on the remaining boundary [9, 69]. (see Figure 5). The physical parameters used are taken from the literature and are listed in Table (2), together with the literature reference specification.

The results of the simulations are reported in Figure 6, which shows us the results for times $t = 0, 12, 15$ and 20 years in a section of the brain. At time $t = 12$ years, we can observe how the atrophy starts when the relative concentration of the misfolded proteins exceeds the critical value c_{crit} . We can observe the presence of a seeding of misfolded τ -proteins located in the amygdala [13, 67]. The proteins spread in all directions according to the axonal directions. The variable g activates later, and the displacement field varies accordingly. At the final time, $T = 20$ years, the concentration of proteins reaches its maximum value in the whole domain, and we can observe a shrinkage of the cortical surface. The dynamic of the relative concentration over the span of 20 years is observed to be coherent with the Braak staging theory [20]. Moreover, the results are coherent with other works in literature on the topic both in terms of prion spreading [44, 6], loss of mass, and atrophy development [9, 53]. We have also observed that the values

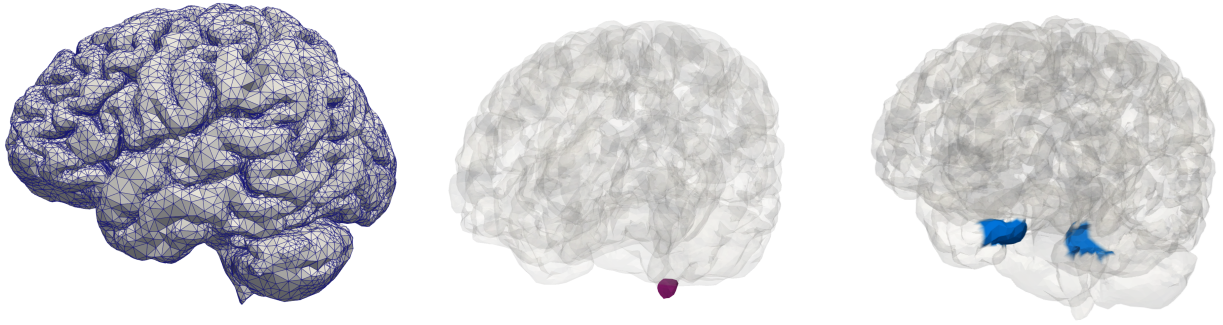


Figure 5: An external representation of the mesh (left), a visualization of the brain stem in purple (center), where we impose homogeneous Dirichlet boundary conditions, and a visualization of the amygdala in blue (right), where the initial concentration of τ -proteins is collocated.

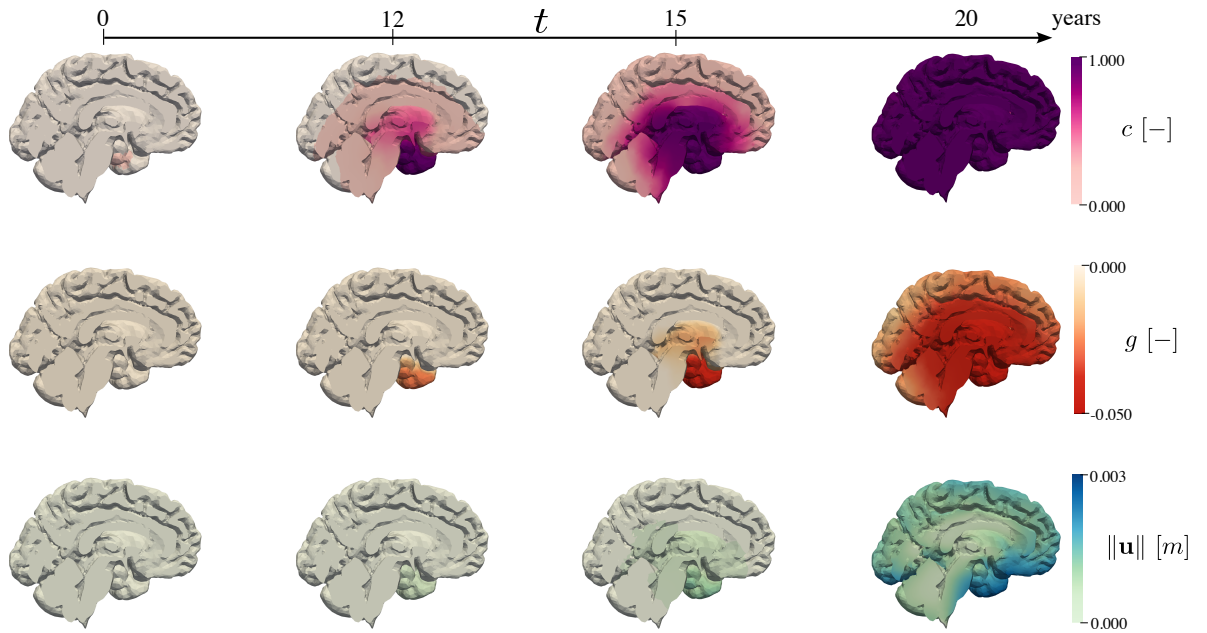


Figure 6: Test Case Section 7. Patterns of tau protein concentration c , atrophy rate g , and displacement \mathbf{u} in Alzheimer's disease simulation at times $t = 0, 12, 15, 20$ years. Results obtained using mesh size $h = 6.23 \times 10^{-3}$ m and polynomial degree $p_c = p_g = p_u = 3$.

of the magnitude of the displacement at final time $T = 20$ years is small, i.e. maximum value equal to 0.003, which further supports the hypothesis of small deformations.

8. Conclusions and further developments

In this work, we have presented a multiphysics model for studying tissue atrophy caused by the spreading of a biological agent, with a specific application to Alzheimer's disease. The agent's spread and aggregation have been modeled using the Fisher-Kolmogorov equation, incorporating both dispersion and proliferation effects. Tissue atrophy has been described through a morpho-elastic framework, where mass loss and tissue elasticity together shape the

Table 3

Parameters used in the test case of Section 8. The references associated with the reference values are reported in the table.

Parameters	Values	Reference	Parameters	Values	Reference
d	8.00 [mm ² /year]	[9]	λ	2700 [Pa]	[51, 52]
α	0.90 [1/year]	[9]	μ	300 [Pa]	[51, 52]
γ	0.20 [–]		\hat{c}	1 [year]	

resulting tissue morphology. The model integrates the morpho-elastic response with the agent's concentration by introducing an evolution law for inelastic strain, governed by the agent concentration through a logistic-type differential equation.

For the construction of the discrete model, we have employed a DG method. We considered a Crank-Nicolson method for the time derivatives discretization and a semi-implicit treatment of the non-linear term. We have assessed the validity of the DG method via two convergence tests, discussing the results with respect to the theoretical outcomes. Secondly, we have validated our method in the coupled case by conducting simulations on a holed-spherical domain. Moreover, we have applied the model to the simulation of Alzheimer's disease on a real brain geometry, where we have observed outcomes consistent with the anticipated biological behavior of prion-like protein diffusion and tissue atrophy.

In the context of neurodegenerative diseases, such as Alzheimer's disease, the model presented in this work is overly simplified, and it would require further development to more precisely represent the onset of the disease. Firstly, concerning protein spreading modeling, a more complex model can be used to capture the diffusion of protein's aggregate of different dimensions, such as the Smoluchowski model [44, 62]. Moreover, this model could capture intermediate states, called oligomers, that seem to be the ones with the highest level of toxicity and so highly correlated with atrophy. Moreover, this could help represent the effects of eventual pharmacological therapy, which can only act on a certain size of oligomeric structures.

Secondly, different atrophy dynamics should be considered. Indeed, the proposed logistic dynamic would have an increase in the atrophy rate in the case of a decrease in the value of c . This property would cause the formation of new mass, which is unphysical. On this side, one could consider the implementation of machine learning strategies to derive a consistent dynamic of the atrophy rate. Indeed, deriving the deformations due to the loss of mass from magnetic resonance images and the associated tau protein concentrations derivable from positron emission tomography (PET), we can learn the functional relation between the quantities, constructing the atrophy rates in a *data-driven* setting. A more detailed mechanistic model of atrophy could be valuable, for example, by incorporating thermodynamic constraints to derive admissible evolution laws, as done in [46]. Nonetheless, a machine learning approach would also be beneficial in this context. Data-driven model discovery is an active area of research in solid mechanics, and its techniques could be meaningfully applied within the framework of our study to select the most appropriate evolution law for Alzheimer's disease-induced atrophy [45].

Concerning the elasticity law, more suitable nonlinear hyperelastic or viscoelastic models can be used to fit brain deformations more accurately, such as the Ogden model, which has been proved to be the best to represent the brain tissue elastic properties [2]. Indeed, while the small elasticity assumption for the whole brain holds due to the relatively low mean value of the atrophy parameter g , some brain regions may experience more significant volume loss. Finally, Robin boundary conditions could be analyzed to take into account the connective tissues that provide support to the brain.

From a numerical point of view, inverse uncertainty quantification strategies can be adopted to calibrate the physical parameters starting from medical images. In particular, PET with appropriate tracers can be used to derive the distribution of misfolded tau protein concentrations in the brain [66]. Then, longitudinal PET studies have been proven to be useful to calibrate the reaction and diffusion parameters in the FK law in Alzheimer's applications [61].

In the next session we present the first numerical results in the framework of non-elasticity model applied to a cubic domain.

8.1. Extension to nonlinear elasticity

As a first step toward the extension to non-linear elasticity, we also perform a simulation incorporating a nonlinear constitutive law for tissue elasticity. In this case, we use discontinuous elements for both the agent's concentration

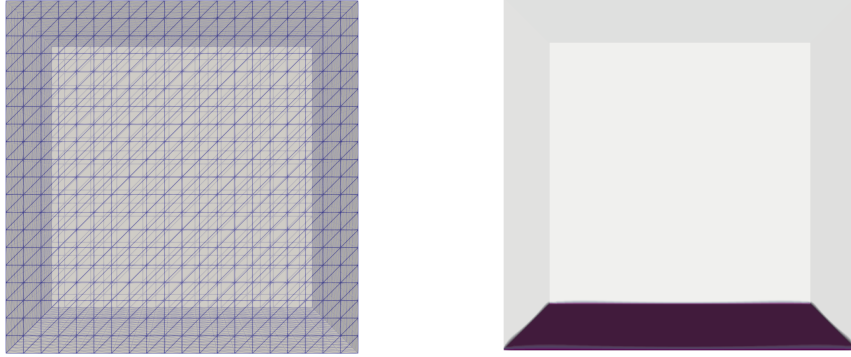


Figure 7: An external representation of the mesh (left) and a visualization of the Dirichlet's boundary in purple and of the Neumann's boundary in transparency (right).

and the atrophy variable g , while opting for continuous elements to discretize the displacement field. We consider the following hyperelastic energy:

$$\Psi_0(\mathbf{F}_E) = \frac{\mu}{2}(\mathbf{F}_E : \mathbf{F}_E - 3 - 2 \log(\det \mathbf{F}_E)) + \frac{\lambda}{2}(\det \mathbf{F}_E - 1)^2.$$

As before, we consider the tensor $\mathbf{G} = (1 + g)\mathbf{I}$. Since small deformations are no longer necessary, we can set the parameter γ (representing the maximum volume loss when the concentration of misfolded tau proteins equals 1) to reach values around 20%. In this case, we have a variation of the volume of the order of $O((1 + g)^3)$. Under such a hypothesis, we do not assume that the current configuration $\Omega_t \equiv \Omega$, the reference configuration.

We consider a cubic domain, denoted as $\Omega = (0 \text{ dm}, 1 \text{ dm})^3$, to be dimensionally coherent with the brain geometry. The parameters are detailed in [6, 7] for the concentration and elasticity equations, as presented in Table 3. Additionally, we enforce a $c_{crit} = 0.8$. Moreover, we define the initial condition as a Gaussian function, ensuring the concentration starts below the critical value:

$$c(\mathbf{X}, 0) = \sqrt{2\pi} \exp \left[-\frac{1}{2} \left(\frac{\mathbf{X} - \mathbf{X}_0}{0.15} \right)^2 \right],$$

where $\mathbf{X}_0 = [0.5 \ 0.5 \ 0.5]^T \text{ dm}$. We take $g(\mathbf{X}, 0) = 0$ as the initial condition for the atrophy field. Finally, we impose homogeneous Dirichlet's boundary conditions on $\Gamma_D^{\mathbf{u}} = [0, 1] \times [0, 1] \times \{Z = 1\}$ along with homogeneous Neumann's conditions on $\Gamma_N^{\mathbf{u}} = \partial\Omega \setminus \Gamma_D^{\mathbf{u}}$, as shown in Figure 7.

We perform the simulations using discontinuous elements for the FK and the logistic equation as in Equation (16) and continuous elements for the nonlinear elasticity equation. In particular, for this simulation, we fix the polynomial degree of the discretization $p_c = p_g = p_{\mathbf{u}} = 2$. The domain is discretized by means of a structured tetrahedral mesh of 48 000 cells ($h = 0.027 \text{ dm}$). The mesh is reported in Figure 7. Concerning the time discretization, we consider a timestep $\Delta t = 10^{-3}$ years and a final time $T = 10$ years.

The results are shown in Figure 8. As expected, we observe that over the years, the biological agent production and diffusion cause the mass loss, initially concentrated in the middle of the cube. After 7 years, we can observe a first macroscopic shrinking of the domain, whose boundaries start deforming. At the final time $T = 10$ years, the maximum theoretical value of the atrophy rate g has been reached in almost all the domain, and the maximum of the deformation is of the order of 20% of the cube edge length. The development of a numerical discretization of the nonlinear elasticity equation with the DG method will be the object of future research. This method would require

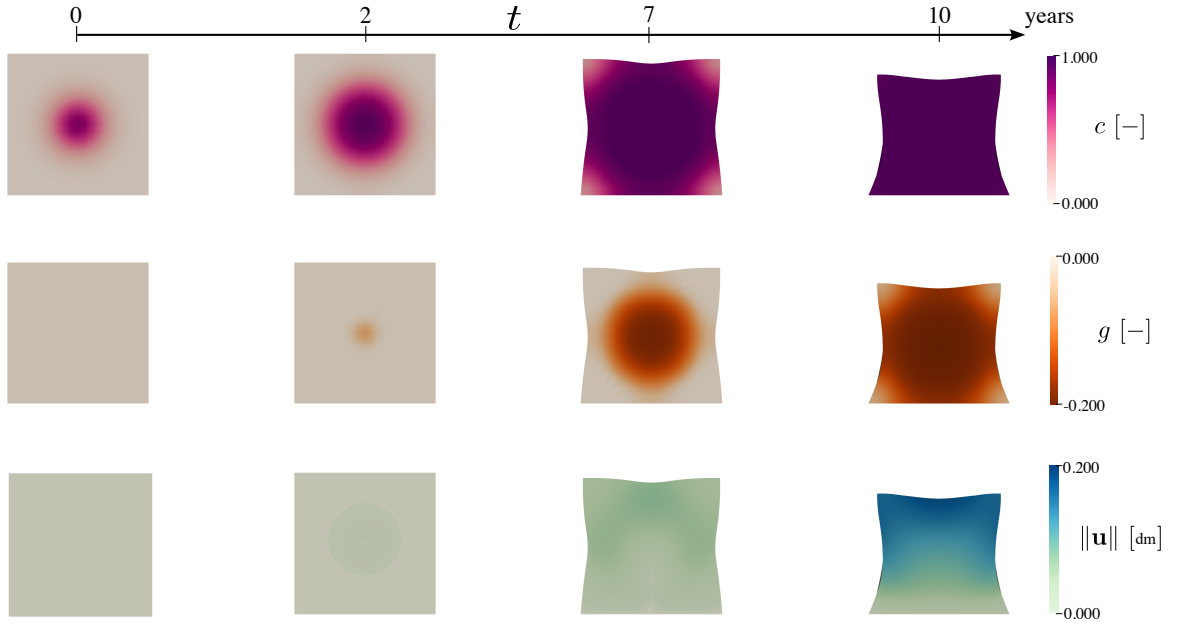


Figure 8: Test Case Section 8. Patterns of concentration c , atrophy rate g , and displacement \mathbf{u} at times $t = 0, 2, 7, 10$ years.

a detailed derivation of the interface integrals, also associated with stabilization provided by the penalty terms, and the corresponding tangent derivatives to implement the Newton iterations that guarantee convergence. In this context, incremental load strategies could be beneficial [63]. However, it allows the extension to polyhedral meshes, which can be used to reduce the computational costs of three-dimensional realistic simulations.

Acknowledgments

The brain MRI images were provided by OASIS-3: Longitudinal Multimodal Neuroimaging: Principal Investigators: T. Benzinger, D. Marcus, J. Morris; NIH P30 AG066444, P50 AG00561, P30 NS09857781, P01 AG026276, P01 AG003991, R01 AG043434, UL1 TR000448, R01 EB009352. AV-45 doses were provided by Avid Radiopharmaceuticals, a wholly-owned subsidiary of Eli Lilly.

A. Appendix A: FK equation in reference configuration

In the current configuration Ω the Fisher-Kolmogorov equation for the concentration of misfolded proteins reads:

$$\frac{\partial c}{\partial t} = \nabla \cdot (\mathbf{D}\nabla c) + \alpha c(1 - c).$$

The integral of a function f in the current configuration is equal to the integral of the same function multiplied for the determinant of the deformation gradient in the reference configuration:

$$\int_{\mathcal{P}_t} f d\mathbf{x} = \int_{\mathcal{P}_0} \mathbf{J} f d\mathbf{X}. \quad (18)$$

Now we consider the partial derivatives:

$$\frac{\partial}{\partial x_i} = \frac{\partial}{\partial X_j} \frac{\partial X_j}{\partial x_i}$$

We define $(\nabla_X)_j$ as $\frac{\partial}{\partial X_j}$, while $\frac{\partial X_j}{\partial x_i}$ is the ij component of the inverse of the deformation gradient \mathbf{F}^{-T} . Indeed, we obtain that:

$$\nabla = \mathbf{F}^{-T} \nabla_X. \quad (19)$$

Now we need to define the divergence operator ($\nabla \cdot$) in the reference configuration. We consider the volume integral over a portion \mathcal{P} of the current configuration of the divergence of a function \mathbf{v} and we apply the divergence theorem:

$$\int_{\mathcal{P}_t} \nabla \cdot \mathbf{v} \, d\mathbf{x} = \int_{\partial\mathcal{P}_t} \mathbf{v} \cdot \mathbf{n} \, ds.$$

Now we apply the Nanson's formula [1]:

$$\int_{\partial\mathcal{P}_t} \mathbf{v} \cdot \mathbf{n} \, ds = \int_{\partial\mathcal{P}_0} \mathbf{v} \cdot (\mathbf{J}\mathbf{F}^{-T}\mathbf{N}) \, dS,$$

then we apply the divergence theorem:

$$\int_{\partial\mathcal{P}_0} \mathbf{v} \cdot (\mathbf{J}\mathbf{F}^{-T}\mathbf{N}) \, dS = \int_{\partial\mathcal{P}_0} (\mathbf{J}\mathbf{F}^{-1}\mathbf{v}) \cdot \mathbf{N} \, dS = \int_{\mathcal{P}_0} \nabla_X \cdot (\mathbf{J}\mathbf{F}^{-1}\mathbf{v}) \, dS. \quad (20)$$

From equations (19), (20) we recovered the expression of the divergence and gradient operators:

$$\nabla \cdot (\mathbf{D}\nabla c) = \nabla_X \cdot (\mathbf{J}\mathbf{F}^{-1}\mathbf{D}\mathbf{F}^{-T}\nabla_X c).$$

With this new expression and with equation (18), we can recover the formulation of the continuous problem in the reference configuration:

$$J \frac{\partial c}{\partial t} = \nabla_X \cdot (\mathbf{J}\mathbf{F}^{-1}\mathbf{D}\mathbf{F}^{-T}\nabla_X c) + \alpha J c (1 - c).$$

B. Appendix B: Derivation of the DG discrete formulation

In this section, we present a more detailed derivation of the DG discretization of our problem. Firstly, we recall that we have defined a partition \mathcal{T}_h of the domain Ω composed of triangular elements $K \in \mathcal{T}_h$. We also recall the definition of the average and jump operator and of the discrete spaces W_h^{DG} , Q_h^{DG} and \mathbf{V}_h^{DG} presented in Section (3). We start by considering the FK problem presented in system (3). We multiply the first equation for a test function $w_h \in W_h^{DG}$ and we integrate it over the partition \mathcal{T}_h :

$$\begin{aligned} \sum_{K \in \mathcal{T}_h} \int_K J \frac{\partial c}{\partial t} w_h \, d\mathbf{X} - \sum_{K \in \mathcal{T}_h} \int_K \mathbf{J}\mathbf{F}^{-1}\mathbf{D}\mathbf{F}^{-T} \Delta c_h w_h \, d\mathbf{X} - \sum_{K \in \mathcal{T}_h} \int_K J \alpha c_h w_h \, d\mathbf{X} + \sum_{K \in \mathcal{T}_h} \int_K J \alpha c_h^2 w_h \, d\mathbf{X} = \\ = \sum_{K \in \mathcal{T}_h} \int_K J f w_h \, d\mathbf{X}. \end{aligned} \quad (21)$$

Now we apply the divergence theorem to the second term of equation (21):

$$- \sum_{K \in \mathcal{T}_h} \int_K \mathbf{J}\mathbf{F}^{-1}\mathbf{D}\mathbf{F}^{-T} \Delta c_h w_h \, d\mathbf{X} = \sum_{K \in \mathcal{T}_h} \int_K \mathbf{J}\mathbf{F}^{-1}\mathbf{D}\mathbf{F}^{-T} \nabla c_h \cdot \nabla w_h \, d\mathbf{X} - \sum_{K \in \mathcal{T}_h} \int_{\partial K} \mathbf{J}\mathbf{F}^{-1}\mathbf{D}\mathbf{F}^{-T} \nabla c_h \cdot \mathbf{n} w_h \, dS.$$

Now, recalling the definition of the jump operator in Section (3), we observe that for two neighboring elements K_1 and K_2 the sum of their boundary integral over their common boundary ∂K_{12} is:

$$\int_{\partial K_{12}} \mathbf{J}\mathbf{F}^{-1}\mathbf{D}\mathbf{F}^{-T} \nabla c_h \cdot \mathbf{n}_{12} w_h \, dS + \int_{\partial K_{12}} \mathbf{J}\mathbf{F}^{-1}\mathbf{D}\mathbf{F}^{-T} \nabla c_h \cdot \mathbf{n}_{21} w_h \, dS = \int_{\partial K_{12}} \llbracket \mathbf{J}\mathbf{F}^{-1}\mathbf{D}\mathbf{F}^{-T} \nabla c_h w_h \rrbracket \, dS, \quad (22)$$

with \mathbf{n}_{12} and \mathbf{n}_{21} , such that $\mathbf{n}_{12} = -\mathbf{n}_{21}$, the outer normals to the elements K_1 and K_2 respectively. From some computations we can derive the following equality [54]:

$$\llbracket c w \rrbracket = \llbracket c \rrbracket \llbracket w \rrbracket + \{c\} \llbracket w \rrbracket. \quad (23)$$

Applying (23) to (22), we obtain:

$$\int_{\partial K_{12}} \llbracket \mathbf{JF}^{-1} \mathbf{DF}^{-T} \nabla c_h w_h \rrbracket dS = \int_{\partial K_{12}} \llbracket \mathbf{JF}^{-1} \mathbf{DF}^{-T} \nabla c_h \rrbracket \llbracket w_h \rrbracket dS + \int_{\partial K_{12}} \llbracket \mathbf{JF}^{-1} \mathbf{DF}^{-T} \nabla c_h \rrbracket \llbracket w_h \rrbracket dS.$$

We observe that for a solution $c \in C^1(\Omega)$ the first integral is equal to 0. Equation (21) then becomes:

$$\begin{aligned} & \sum_{K \in \mathcal{T}_h} \int_K J \frac{\partial c}{\partial t} w_h d\mathbf{X} + \sum_{K \in \mathcal{T}_h} \int_K \mathbf{JF}^{-1} \mathbf{DF}^{-T} \nabla c_h \cdot \nabla w_h d\mathbf{X} - \sum_{F \in \mathcal{F}_h^I} \int_F \llbracket \mathbf{JF}^{-1} \mathbf{DF}^{-T} \nabla c_h \rrbracket \llbracket w_h \rrbracket dS \\ & - \sum_{F \in \mathcal{F}_h^B} \int_F \mathbf{JF}^{-1} \mathbf{DF}^{-T} \nabla c_h \cdot \mathbf{n} w_h dS - \sum_{K \in \mathcal{T}_h} \int_K J \alpha c_h w_h d\mathbf{X} + \sum_{K \in \mathcal{T}_h} \int_K J \alpha c_h^2 w_h d\mathbf{X} = \sum_{K \in \mathcal{T}_h} \int_K J f w_h d\mathbf{X} \end{aligned}$$

Since we have homogeneous Neumann boundary conditions the integral over the boundary faces is null. The discrete problem now reads: Find $c_h \in W_h^{DG}$ such that:

$$\begin{aligned} & \sum_{K \in \mathcal{T}_h} \int_K J \frac{\partial c}{\partial t} w_h d\mathbf{X} + \sum_{K \in \mathcal{T}_h} \int_K \mathbf{JF}^{-1} \mathbf{DF}^{-T} \nabla c_h \cdot \nabla w_h d\mathbf{X} - \sum_{F \in \mathcal{F}_h^I} \int_F \llbracket \mathbf{JF}^{-1} \mathbf{DF}^{-T} \nabla c_h \rrbracket \llbracket w_h \rrbracket dS \\ & - \sum_{K \in \mathcal{T}_h} \int_K J \alpha c_h w_h d\mathbf{X} + \sum_{K \in \mathcal{T}_h} \int_K J \alpha c_h^2 w_h d\mathbf{X} = \sum_{K \in \mathcal{T}_h} \int_K J f w_h d\mathbf{X} \quad \forall w_h \in W_h^{DG} \end{aligned}$$

Additionally, to ensure symmetry the problem we subtract the term:

$$\sum_{F \in \mathcal{F}_h^I} \int_F \llbracket c_h \rrbracket \llbracket \mathbf{JF}^{-1} \mathbf{DF}^{-T} \nabla w_h \rrbracket dS.$$

This formulation is then called Symmetric Interior Penalty (SIP) [65]. Moreover, we add a stabilization term:

$$\sum_{F \in \mathcal{F}_h^I} \eta \llbracket c_h \rrbracket \cdot \llbracket w_h \rrbracket dS,$$

where η is a penalty, defined as in the first definition of (15), term suitably chosen. In a very similar way, it is also possible to recover the DG discretization for the logistic equation and for the elasticity equation.

C. Appendix C: Dependence of atrophy function on the parameter β

To show the role of $g = g(t)$, we have also reported three different graphs of the function for different values of β , see Figure (9). Please note that these behaviors are local both in space and time since the parameter β strongly depends on the concentration's values, but here we consider β to be constant to give an idea of what the behavior of the atrophy g is.

References

- [1] R. W. Ogden, Non-linear elastic deformations, Courier Corporation, 1997.
- [2] S. Budday, G. Sommer, C. Birkl, C. Langkammer, J. Haybaeck, J. Kohnert, M. Bauer, F. Paulsen, P. Steinmann, E. Kuhl, G. A. Holzapfel, Mechanical characterization of human brain tissue, *Acta biomaterialia* 48 (2017) 319–340.
- [3] A. Schäfer, P. Chaggar, T. B. Thompson, A. Goriely, E. Kuhl, Predicting brain atrophy from tau pathology: a summary of clinical findings and their translation into personalized models, *Brain Multiphysics* 2 (2021) 100039.
- [4] M. E. Gurtin, E. Fried, L. Anand, The mechanics and thermodynamics of continua, Cambridge university press, 2010.
- [5] E. K. Rodriguez, A. Hoger, A. D. McCulloch, Stress-dependent finite growth in soft elastic tissues, *Journal of biomechanics* 27 (1994) 455–467.
- [6] M. Corti, F. Bonizzoni, L. Dedé, A. M. Quarteroni, P. F. Antonietti, Discontinuous Galerkin methods for Fisher-Kolmogorov equation with α -synuclein spreading in Parkinson's disease, *Computer Methods in Applied Mechanics and Engineering* 417 (2023) 116450.
- [7] M. Corti, L. Dedé, A. M. Quarteroni, P. F. Antonietti, Numerical Modelling of the Brain Poromechanics by Higher-Order Discontinuous Galerkin Methods, *Mathematical Models and Methods in Applied Sciences* 33 (2023) 1577–1609.

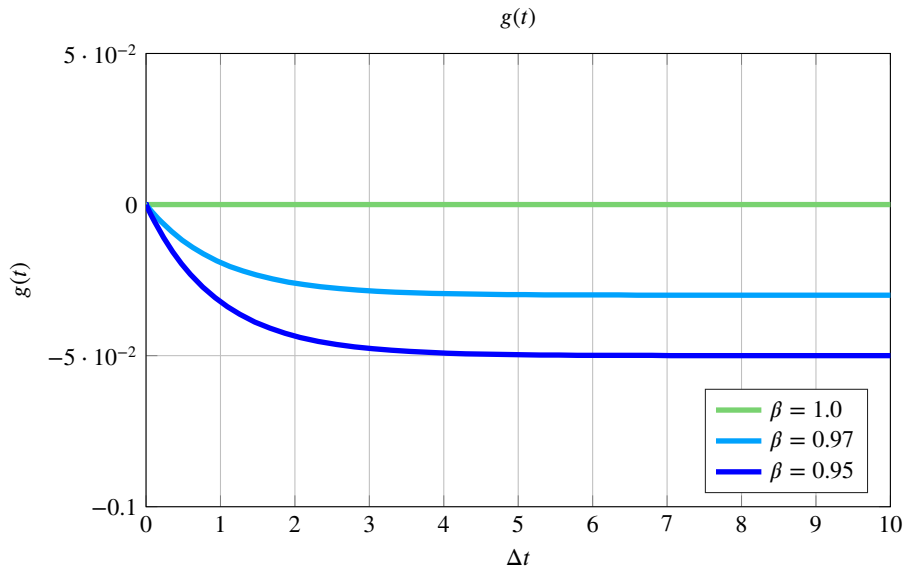


Figure 9: Three different plots for the atrophy function $g(t)$ for three different values of $\beta = 1$ (decoupled system), $\beta = 0.97$ (intermediate case), $\beta = 0.95$ (minimum value of β , when considering linear elasticity obtained from $\beta = 1 - \gamma$, with $\gamma = 0.05$ in Table 1, suitable value for small deformation assumption).

- [8] P. F. Antonietti, F. Bonizzoni, M. Corti, A. Dall'Olio, Discontinuous Galerkin approximations of the heterodimer model for protein-protein interaction, *Computer Methods in Applied Mechanics and Engineering* 431 (2024) 117282.
- [9] A. Schäfer, J. Weickenmeier, E. Kuhl, The interplay of biochemical and biomechanical degeneration in Alzheimer's disease, *Computer Methods in Applied Mechanics and Engineering* 352 (2019) 369–388.
- [10] S. Fornari, A. Schäfer, E. Kuhl, A. Goriely, Spatially-extended nucleation-aggregation-fragmentation models for the dynamic of prion-like neurodegenerative protein-spreading in the brain and its connectome, *Journal of Theoretical Biology* 486 (2020) 110102.
- [11] M. S. Alnaes, J. Blechta, J. Hake, A. Johansson, B. Kehlet, A. Logg, C. N. Richardson, J. Ring, M. E. Rognes, G. N. Wells, The FEniCS project version 1.5, *Archive of Numerical Software* 3 (2015).
- [12] A. Goriely, *The Mathematics and Mechanics of Biological Growth*, Springer New York, NY, 2017.
- [13] M. Jucker, L. C. Walker, Self-propagation of pathogenic protein aggregates in neurodegenerative diseases, *Nature* 501 (2013) 45–51.
- [14] M. E. Gurtin, *An Introduction on Continuum Mechanics*, Academic Press, 1981.
- [15] D. A. D. Pietro, J. Droniou, *The Hybrid High-Order Method for Polytopal Meshes: Design, Analysis, and Applications*, Springer International Publishing, 2020.
- [16] S. Salsa, G. Verzini, *Partial Differential Equations in Action: From Modelling to Theory*, Springer, 2022.
- [17] S. Salsa, *Equazioni a derivate parziali*, Springer, 2016.
- [18] Q. A. M., *Numerical Models for Differential Problems*, Springer, 2016.
- [19] WHO, Dementia, 2023. <https://www.who.int/news-room/fact-sheets/detail/dementia>.
- [20] H. Braak, E. Braak, Neuropathological stages of Alzheimer-related changes, *Acta Neuropathologica* 82 (1991) 239–259.
- [21] V. L. Villemagne, S. Burnham, P. Bourgeat, B. Brown, K. A. Ellis, O. Salvado, C. Szoek, S. L. Macaulay, R. Martins, P. Maruff, D. Ames, C. C. Rowe, C. L. Masters, Amyloid β deposition, neurodegeneration, and cognitive decline in sporadic Alzheimer's disease: a prospective cohort study, *The Lancet, Neurology* 12 (2013) 357–367.
- [22] S. B. Prusiner, Prions, Nobel Lecture, *Proc. Natl. Acad. Sci. USA* 95 (1998).
- [23] M. Jucker, L. C. Walker, Self-propagation of pathogenic protein aggregates in neurodegenerative diseases, *Nature* 501 (2013) 45–51.
- [24] M. Jucker, L. C. Walker, Propagation and spread of pathogenic protein assemblies in neurodegenerative diseases, *Nature Neuroscience* 21 (2018) 1341–1349.
- [25] B. B. Holmes, M. I. Diamond, Prion-like properties of tau proteins: the importance of extracellular tau as a therapeutic target, *The Journal of Biological Chemistry* 289 (2014).
- [26] G. F. Hall, B. A. Patuto, Is tau ready for the admission to the prion club, *Prion* 6 (2012).
- [27] J. Weickenmeier, E. Kuhl, A. Goriely, Multiphysics of prionlike diseases: Progression and atrophy, *Physical Review Letters* 121 (2018) 158101.
- [28] G. B. Stokin, Axonal transport and Alzheimer's disease, *Annual Review of Biochemistry* 75 (2006).
- [29] W. Schiesser, *ODE/PDE α -synuclein models for Parkinson's disease*, 1 ed., Elsevier, 2018. doi:<https://doi.org/10.1016/C2017-0-01259-4>.
- [30] O. Camara, M. Schweiger, R. I. Scahill, W. R. Crum, Phenomenological model of diffuse global and regional atrophy using finite-element methods, *IEEE Transactions on Medical Imaging* 25 (2006).

- [31] R. Ashish, A. Kuceyeski, M. Weiner, A network diffusion model of disease progression in dementia, *Neuron* 73 (2012).
- [32] F. Bassi, L. Botti, A. Colombo, D. A. Di Pietro, P. Tesini, On the flexibility of agglomeration based physical space discontinuous Galerkin discretizations, *Journal of Computational Physics* 231 (2012) 45–65.
- [33] P. F. Antonietti, N. Farenga, E. Manuzzi, G. Martinelli, L. Saverio, Agglomeration of polygonal grids using graph neural networks with applications to multigrid solvers, *Computers & Mathematics with Applications* 154 (2024).
- [34] J. S. Hesthaven, T. Warburton, *Nodal Discontinuous Galerkin Method: Algorithms, Analysis and Applications*, Springer International Publishing, 2008.
- [35] P. F. Antonietti, C. Facciola, P. Houston, I. Mazzieri, G. Pennesi, M. Verani, High-order Discontinuous Galerkin Methods on Polyhedral Grids for Geophysical Applications: Seismic Wave Propagation and Fractured Reservoir Simulations, in: *Polyhedral Methods in Geosciences*, Springer International Publishing, 2021, pp. 159–225.
- [36] A. Cangiani, Z. Dong, E. Georgoulis, P. Houston, *hp-Version Discontinuous Galerkin Methods on Polygonal and Polyhedral Meshes*, Springer, 2017.
- [37] J. Keener, J. Sneyd, *Mathematical Physiology I: Cellular Physiology*, Springer Science+Business Media, 2009.
- [38] R. Fisher, The wave of advance of advantageous genes, *Annals of Eugenics* 7 (1937) 353–369.
- [39] E. Kuhl, Growing matter: a review of growth in living systems, *Journal of the mechanical behaviour of biomedical materials* 29 (2014).
- [40] B. J. Walker, G. L. Celora, A. Goriely, D. E. Moulton, H. M. Byrne, Minimal morphoelasticity models of solid tumour spheroids: a tutorial, *Bulletin of Mathematical Biology* 85 (2023).
- [41] D. Ambrosi, G. Ateshian, A. E.M., S. C. Cowin, J. Dumais, A. Goriely, G. Holzapfel, J. Humphrey, E. Kemkemer, R. Kuhl, J. Olberding, L. Taber, K. Garikipati, Perspectives on biological growth and remodeling, *Journal of Mechanics and Physics of Solids* 59 (2011) 863–883.
- [42] S. Fornari, A. Schäfer, M. Jucker, A. Goriely, E. Kuhl, Prion-like spreading of Alzheimer's disease within the brain connectome, *Journal of The Royal Society Interface* 16 (2019) 20190356.
- [43] P. LaMontagne, T. L. Benzinger, J. Morris, S. Keefe, R. Hornbeck, C. Xiong, E. Grant, J. Hassenstab, K. Moulder, A. Vlassenko, M. Raichle, C. Cruchaga, D. Marcus, OASIS-3: Longitudinal Neuroimaging, Clinical, and Cognitive Dataset for Normal Aging and Alzheimer Disease, *medRxiv* (2019).
- [44] J. Weickenmeir, M. Jucker, A. Goriely, E. Kuhl, A physics-based model explains the prion-like features of neurodegeneration in alzheimer's disease, parkinson's disease, and amyotrophic lateral sclerosis, *Journal of the Mechanics and Physics of Solids* 124 (2019) 264–281.
- [45] M. Flaschel, S. Kumar, L. De Lorenzis, Unsupervised discovery of interpretable hyperelastic constitutive laws, *Computer Methods in Applied Mechanics and Engineering* 381 (2021) 113852.
- [46] D. Ambrosi, F. Guana, Stress-modulated growth, *Mathematics and mechanics of solids* 12 (2007) 319–342.
- [47] J. Belmonte-Betia, G. Calvo, V. Pérez-García, Effective particle methods for Fisher-Kolmogorov equations: Theory and applications to brain tumor dynamics, *Communication in Nonlinear Science and Numerical Simulations* 19 (2014) 3267–3283.
- [48] M. Bertsch, B. Franchi, L. Meacci, M. Primicerio, M. Tesi, The amyloid cascade hypothesis and Alzheimer's disease: A mathematical model, *European Journal of Applied Mathematics* 32 (2020).
- [49] A. N. Kolmogorov, I. G. Petrovskii, N. S. Piskunov, Etude de la diffusion avec croissance de la quantité de matière et son application à un problème biologique, *Moscow University Mathematics Bulletin* 1 (1937) 1–25.
- [50] M. Corti, Exploring tau protein and amyloid-beta propagation: A sensitivity analysis of mathematical models based on biological data, *Brain Multiphysics* 7 (2024).
- [51] E. Griffiths, J. Hinrichsen, N. Reiter, S. Budday, On the importance of using region-dependent material parameters for full-scale human brain simulations, *European Journal of Mechanics - A/Solids* 99 (2023) 104910.
- [52] J. Hinrichsen, N. Reiter, L. Brüer, F. Paulsen, S. Kaessmair, S. Budday, Invaders identification of region-specific hyperelastic material parameters for human brain tissue, *Biomechanics and Modeling in Mechanobiology* 22 (2023) 1729–1749.
- [53] B. Y., J. Weickenmeir, Brain Shape Changes Associated with General Atrophy in Healthy Aging and Alzheimer's Disease, *Frontiers in Medical Engineering* 7 (2021).
- [54] D. Arnold, F. Brezzi, B. Cockburn, L. Marini, Unified Analysis of Discontinuous Galerkin Methods for Elliptic Problems, *Journal on Numerical Analysis* 39 (2002).
- [55] D. Perl, Neurophatology of Alzheimer's disease, *Mount Sinai Journal of Medicine* 77 (2010) 32–42.
- [56] P. Amestoy, I. S. Duff, J. Koster, J.-Y. L'Excellent, A fully asynchronous multifrontal solver using distributed dynamic scheduling, *SIAM Journal on Matrix Analysis and Applications* 23 (2001) 15–41.
- [57] H. Zheng, H. Sum, Q. Cai, H. Tai, The Enigma of Tau Protein Aggregation: Mechanistic Insights and Future Challenges, *International Journal of Molecular Science* 25 (2024).
- [58] A. Logg, K. Mardal, G. Wells, *Automated Solution of Differential Equations by the Finite Element Method*, Springer Publishing Company, Incorporated, 2012.
- [59] M. Brett, C. Markiewicz, M. Hanke, M.-A. Côté, B. Cipollini, P. McCarthy, C. Cheng, Nibabel 4.0.0: Access a cacophony of neuro-imaging file formats, 2022. URL: <https://github.com/nipy/nibabel>.
- [60] K.-A. Mardal, M. E. Rognes, T. B. Thompson, L. Magnus Valnes, *Mathematical Modeling of the Human Brain – From Magnetic Resonance Images to Finite Element Simulation*, Springer, 2021.
- [61] M. Corti, F. Bonizzoni, P. F. Antonietti, A. M. Quarteroni, Uncertainty quantification for Fisher-Kolmogorov equation on graphs with application to patient-specific Alzheimer's disease, *ESAIM: Mathematical Modelling and Numerical Analysis* 58 (2024) 2135–2154.
- [62] B. Franchi, S. Lorenzani, Homogenization of Smoluchowski-type equations with transmission boundary conditions, *Advanced Nonlinear Studies* 24 (2024) 952–991.
- [63] L. Botti, L. Verzeroli, BR2 discontinuous Galerkin methods for finite hyperelastic deformations, *Journal of Computational Physics* 463 (2022) 111303.

- [64] A. M. Dale, B. Fischl, M. I. Sereno, Cortical surface-based analysis: I. segmentation and surface reconstruction, *NeuroImage* 9 (1999) 179–194.
- [65] D. N. Arnold, An Interior Penalty Finite Element Method with Discontinuous Elements, *SIAM Journal on Numerical Analysis* 19 (1982) 742–760. Publisher: Society for Industrial and Applied Mathematics.
- [66] W. M. van Oostveen, E. C. M. de Lange, Imaging techniques in Alzheimer's disease: a review of applications in early diagnosis and longitudinal monitoring, *International Journal of Molecular Sciences* 22 (2021) 2110.
- [67] P. T. Nelson, E. L. Abner, E. Patel, S. Anderson, D. M. Wilcock, R. J. Kryscio, L. J. Van Eldik, G. A. Jicha, Z. Gal, R. S. Nelson, B. G. Nelson, J. Gal, T. Azam, D. W. Fardo, M. Cykowski, The amygdala as a locus of pathologic misfolding in neurodegenerative diseases, *Journal of Neuropathology & Experimental Neurology* 77 (2017) 2–20.
- [68] A. Ern, A. F. Stephansen, P. Zunino, A discontinuous galerkin method with weighted averages for advection–diffusion equations with locally small and anisotropic diffusivity, *IMA Journal of Numerical Analysis* 29 (2008) 235–256.
- [69] T. C. Harris, R. de Rooij, E. Kuhl, The Shrinking Brain: Cerebral Atrophy Following Traumatic Brain Injury, *Annals of Biomedical Engineering* 47 (2019) 1941–1959. Number: 9.